UC Irvine

UC Irvine Electronic Theses and Dissertations

Title

BRET-based reporter conjugated luminescent nanoparticles for improved bioluminescence imaging

Permalink

https://escholarship.org/uc/item/0m80v11j

Author

Tahir, Mahum

Publication Date

2023

Peer reviewed|Thesis/dissertation

UNIVERSITY OF CALIFORNIA,
IRVINE

BRET-based reporter conjugated luminescent nanoparticles
for improved bioluminescence imaging

THESIS

Submitted in partial satisfaction of the requirements
for the degree of

MASTER OF SCIENCE

in Biomedical Engineering

by

Mahum Tahir

Thesis Committee:
Professor Szu-Wen Wang, Chair
Professor Elliot Botvinick
Professor Wendy Liu

2023

TABLE OF CONTENTS

LIST OF FIGURES

LIST OF TABLES

LIST OF ABBREVIATIONS USED

BLI: bioluminescence imaging

Fluc: Firefly luciferase

Rluc: *Renilla* luciferase

Nluc: nanoluciferase

CTZ: coelenterazine

FRZ: furimazine

DTZ: diphenylterazine

BRET: bioluminescence resonance energy transfer

SC: SpyCatcher

ST: SpyTag

PCR: polymerase chain reaction

PBS: phosphate buffered saline

DLS: dynamic light scattering

SEM: standard error of mean

ACKNOWLEDGEMENTS

I would like to acknowledge all those who helped and supported me during my Master's program at UCI. I would like to express my deepest gratitude to my advisor, Dr. Szu-Wen Wang, for allowing me to conduct research in her lab and for her continuous guidance and mentorship throughout my research journey. I would also like to thank all my lab mates for giving me helpful advice throughout my research. I would especially like to thank Enya Li for her valuable insights and feedback throughout the ups and downs of my project. I gained invaluable skills and knowledge during graduate school that I will carry with me in my future career.

Lastly, I would like to express my appreciation to my parents, family, and friends for their continuous support and encouragement throughout my graduate school journey.

ABSTRACT OF THE THESIS

BRET-based reporter conjugated luminescent nanoparticles

for improved bioluminescence imaging

By

Mahum Tahir

Master of Science in Biomedical Engineering

University of California, Irvine, 2023

Professor Szu-Wen Wang, Chair

The emergence of bright bioluminescent luciferase reporters has enabled versatile bioimaging applications *in vitro* and *in vivo*. However, conventional luciferases such as nanoluciferase are sub-optimal reporters for bioluminescence imaging (BLI) *in vivo* due to their blue-shifted emission which is highly attenuated by tissue, resulting in a dim, less sensitive signal. To overcome this limitation, Nluc and its substrate furimazine have been further engineered to produce red-shifted emission. Additionally, Nluc has been fused to fluorescent proteins, creating reporters with spectrally shifted light emission through bioluminescence resonance energy transfer (BRET). In this study, we employed two BRET-based fusion reporters, CeNLuc and LumiScarlet, as they have previously demonstrated improved imaging properties compared to luciferase-only reporters. We aimed to immobilize CeNLuc and LumiScarlet onto the E2 nanoparticle surface to develop brighter reporters for BLI. We successfully conjugated CeNLuc and LumiScarlet onto E2 using the SpyCatcher-SpyTag conjugation, resulting in CeNLuc-E2 and LumiScarlet-E2 nanoparticles of ~35-nm in size. Furthermore, we were able to control the number of luminescent proteins per particle and demonstrated that CeNLuc-E2 and LumiScarlet-E2 underwent efficient BRET. We also evaluated the luminescence of CeNLuc-E2

and LumiScarlet-E2 using BLI. CeNLuc-E2 particles produced approximately 12-fold greater luminescence than non-immobilized CeNLuc proteins, resulting in a brighter luminescent reporter. In contrast, LumiScarlet-E2 particles exhibited a greater red-shifted emission than CeNLuc-E2, which could be advantageous for more sensitive deep-tissue BLI. These findings demonstrate the potential of CeNLuc-E2 and LumiScarlet-E2 as effective reporters for broad applications in nanomedicine and bioimaging.

1. INTRODUCTION AND BACKGROUND

1.1. Introduction

Bioluminescence imaging (BLI) has become a powerful technique for visualizing biological processes at the cellular, tissue, and organism level. This is primarily attributed to the advances made in the discovery and optimization of bright bioluminescent reporter systems [1]. Bioluminescence is a result of a chemical reaction between an enzyme called a luciferase and a substrate called a luciferin [2]. The luciferase catalyzes the oxidation of luciferin, which results in oxyluciferin and the production of light (Figure 1) [3]. Bioluminescence has many advantages over other imaging modalities, such as fluorescence, including a better signal-to-noise ratio and lower background, enabling highly sensitive imaging [4]. Moreover, bioluminescence requires no excitation light, avoiding concerns related to fluorophore photobleaching or tissue autofluorescence during imaging [5]. As a result, bioluminescence has become a valuable tool for noninvasive *in vivo* imaging applications. Bioluminescent emission can be visualized using sensitive charge-coupled device (CCD) cameras to monitor processes such as protein-protein interactions, gene expression, cell migration and biodistribution *in vivo* [6,7]. However, due to the dim signal of luciferases, bioluminescence is still limited in imaging deep tissues [8,9]. Thus, there still exists a need for bioluminescent reporters that are brighter and possess improved tissue penetration for *in vivo* imaging. In this section, more background is presented on current bioluminescent reporters used for *in vivo* BLI, their limitations in deep tissue imaging and other strategies being employed to improve bioluminescence detection *in vivo*.

1.2. Bioluminescence-based reporters for *in vivo* BLI

Conventional luciferases used in bioimaging include the Firefly luciferase (Fluc) and *Renilla* luciferase (Rluc), both of which are commercially available [10,11]. However, these

luciferases can be suboptimal for reporter assays due to their large size (>35 kDa) and their dim

signal, especially *in vivo* [2]. Furthermore, Fluc requires cofactors such as ATP to activate the

substrate, D-luciferin, which results in metabolic disruption in cells, making it unsuitable to use

in vivo [12]. Rluc, however, does not require ATP to produce light, yet its substrate

coelenterazine (CTZ) is unstable in serum and has poor water solubility, limiting its use *in vivo*

[10].
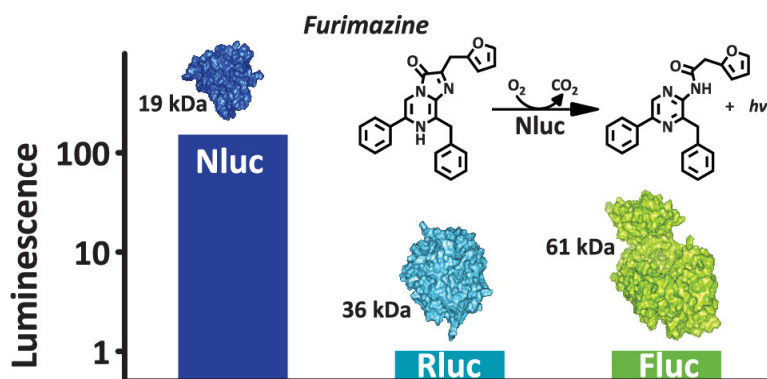
Figure 1. The bioluminescence reaction between Nluc and its substrate furimazine. Nluc is a
smaller and brighter protein compared to other conventional luciferases such as Rluc-CTZ and
Fluc-D-Luciferin. Adapted from Hall 2012 [13].

Recently, the nanoluciferase (Nluc) enzyme has been developed commercially and gained

popularity in bioluminescence applications. Nuc is a small protein (19.1 kDa) that has been

optimized for a substrate called furimazine (FRZ) [13]. The Nluc-FRZ reaction produces

luminescence that is about 150 times greater than Fluc and Rluc, making it one of the brightest

luminescence reporters available (Figure 1) [14]. Nluc has been successfully used for *in vivo* BLI

applications such as imaging superficial tumors and organs [2]. However, for deep tissue

applications such as imaging deep tumors, tracking tumor progression or cell migration, it has

shown reduced sensitivity and a reduced spatiotemporal resolution *in vivo* [2]. Although Nluc

produces an intense light output, it has a blue-shifted emission that peaks around 440 to 460 nm

[14]. This blue emission is a drawback of Nluc because short-wavelength light, such as blue and green light (<600 nm), is highly absorbed by hemoglobin and scattered by tissue [15], limiting the deep tissue penetration of Nluc bioluminescence. In contrast, red-shifted light, greater than 600 nm, is less attenuated by tissue and can penetrate through increased tissue depths [16]. To enhance the performance of Nluc-FRZ for *in vivo* imaging, attempts have been made to modulate the substrate to produce red-shifted emission, yet this often results in a reduced Nluc intensity [12]. As a result, Nluc has also been engineered to produce brighter luminescence when paired with other substrates.

More recently, Nluc has been mutated to create teLuc, which has been modulated for a CTZ analog called diphenylterazine (DTZ) [9]. The teLuc-DTZ reaction produces about 2.6-fold greater luminescence than Nluc-FRZ, with an emission peak around 502 nm. Furthermore, teLuc-DTZ demonstrated about 7.5-fold greater intensity than Nluc-FRZ for *in vivo* BLI, owing to its enhanced luminescence and less blue-shifted emission [9]. However, FRZ, DTZ, and CTZ are known to have low solubility at high concentrations *in vivo*, so small animals can tolerate only small volumes of substrate injection [12]. To address this, DTZ was chemically modified to improve its water solubility, resulting in 8pyDTZ. In solubility assays, 8pyDTZ demonstrated ~13-fold enhanced solubility than DTZ [12]. The teLuc luciferase was further modified to LumiLuc, to optimize it for increased luminescence with the 8pyDTZ substrate [12]. LumiLuc-8pyDTZ produced an emission around 525 nm and displayed bright signals *in vitro* as well as high-sensitivity in an *in vivo* tumor model [12]. Furthermore, the red-shifted luminescence of LumiLuc and high solubility of 8pyDTZ, could make LumiLuc-8pyDTZ a more ideal bioluminescent reporter than Nluc-FRZ for *in vivo* BLI.

1.3. BRET-based luminescent reporters for more enhanced *in vivo* BLI

Another strategy to develop brighter or more red-shifted bioluminescent reporters for *in vivo* BLI is through bioluminescence resonance energy transfer (BRET) [17,18]. BRET involves the transfer of non-radiative energy from a luminescent donor molecule to a fluorescent acceptor molecule [19]. The luciferase-luciferin reaction results in the production of bioluminescence, which serves as an excitation source for a fluorophore molecule to emit light at its emission wavelength [20,21]. This process only occurs if the two molecules are in close proximity (<10 nm) to each other [21] (Figure 2). The efficiency of BRET is affected by several factors, including the distance between the donor and acceptor, the quantum yield of the donor molecule, and the spectral overlap between the donor emission and acceptor excitation [21,22]. Luciferases have been directly fused to fluorophores to create reporters that luminesce through BRET due to their close proximity [5,23,24]. Moreover, the emission of these BRET-based reporters can be spectrally tuned by pairing luciferases to fluorophores of differing emission wavelengths [5]. Therefore, different combinations of luminescent and fluorescent proteins have been engineered and assayed to find the most efficient BRET-fusion pairs.
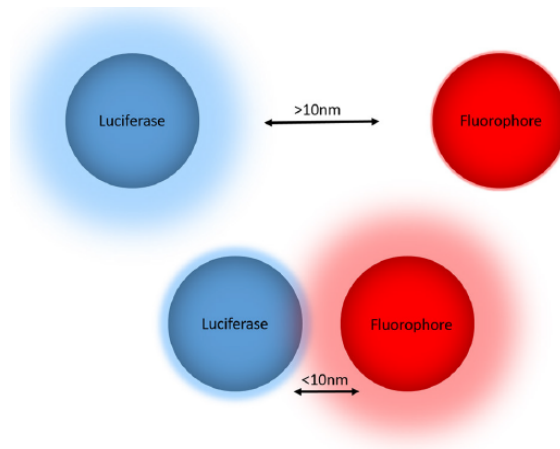

Figure 2. The process of BRET. BRET from the luciferase to the fluorophore can only occur when both molecules are within <10 nm of each other. Adapted from Dale 2019.

Nluc and its derivatives make for optimal donors for BRET-based reporters due to their small size and enhanced light output [17]. Nluc has been fused to a multitude of fluorescent proteins, resulting in a vast library of BRET-based reporters that undergo efficient energy transfer and produce signals brighter than Nluc alone. These include reporters such as GpNluc, GeNL, and CeNLuc [5,25,26]. LumiLuc and teLuc have also been fused to fluorescent proteins to produce BRET-based reporters that are bright and red-shifted, such as LumiScarlet and Antares2, respectively [9,12]. BRET-activated reporters have been effectively utilized for *in vitro* and *in vivo* BLI applications, such as monitoring molecular interactions or tracking tumor progression [14]. Furthermore, BRET-based reporters show greater effectiveness than luciferase reporters for more sensitive *in vivo* BLI [12,24].

1.4. Luminescent nanoparticles for *in vivo* BLI

Bioluminescent and BRET-activated luminescent nanoparticles have also been explored for *in vivo* BLI. In addition to bioimaging, luminescent nanoparticles have been utilized for nanomedicine applications such as monitoring the pharmacokinetics of drug-based nanocarriers or tracking the biodistribution of particles *in vivo* [1,27]. Recently, our lab has assembled Nluc onto a protein nanoparticle platform, E2, to produce luminescent Nluc-E2 nanoparticles for bioimaging [28]. Studies have shown that immobilizing enzymes onto large protein assemblies can enhance the overall catalytic activity of enzymes [29]. Increased catalytic activity could be due to an increase in the localized density of enzymes when they are conjugated to a nanoparticle surface versus when enzymes are free in solution [30]. Additionally, enzymes could be conjugated to a surface in a way that orients their substrate binding pocket in an orientation that is more accessible to substrates increasing their catalytic efficiency [30]. Thus, it was hypothesized that Nluc-E2 could be an even brighter luminescent reporter than Nluc because

Nluc immobilized on E2 could undergo enhanced luciferase performance than unconjugated Nluc, thus outputting more light. In fact, Nluc-E2 showed an 11-fold greater luminescence compared to free Nluc *in vitro* [28]. Furthermore, the biodistribution of Nluc-E2 was tracked *in vivo* and showed higher signal-to-noise ratios than a conventional imaging reporter model of fluorescently labeled E2, demonstrating Nluc-E2 enables more sensitive *in vivo* imaging [28]. The Nluc-E2 imaging platform could be further modulated to improve bioimaging by the assembly of brighter or more red-shifted reporters onto the particle.

As mentioned earlier, Nluc is a sub-optimal reporter for deep tissue imaging as its blue emission is highly absorbed, limiting its tissue penetration and reducing its spatial resolution. Thus, BRET has also been utilized to produce BRET-activated luminescent nanoparticles with red-shifted emission for BLI [1]. More commonly, luciferases have been assembled directly onto the surface of various quantum dot (QD) nanoparticles that produce light when excited [1,31,32] (Figure 3). For example, Nluc was conjugated to the red-shifted QD705 to make QD-Nluc. Once furimazine was administered, Nluc emitted light which then excited QD705 to emit light through BRET. QD-Nluc was used to image tumors and lymph nodes *in vivo* and enabled bioimaging with high signal-to-noise ratios [31]. QD platforms, however, can induce toxicity in cells at high doses and can aggregate in blood, limiting their use for effective *in vivo* BLI [33,34]. Luciferases have also been conjugated to the surfaces of polymer or lipid nanoparticles that are loaded with fluorescent molecules [1]. These particles can produce BRET-based luminescence that is red-shifted for bioimaging [35] (Figure 3). Yet, the BRET efficiency can be decreased due to the increased distance between the luciferases and fluorophores, resulting in the loss of some luminescence [31].
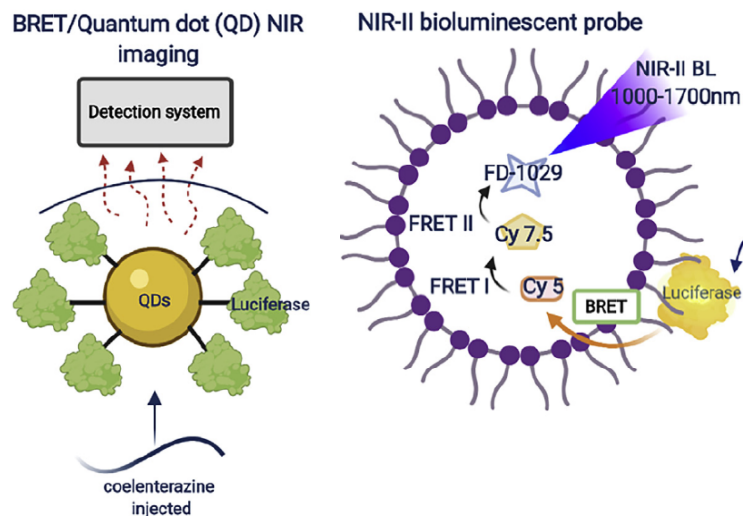
Figure 3. BRET-activated luminescent nanoparticle designs. Common BRET-based particles comprise luciferases conjugated to QD nanoparticles, which emit light when excited by the luciferase through BRET (left). Another BRET-based particle design comprises luciferases surface-conjugated to particles internally loaded with fluorescent molecules (right). When the luciferase bioluminesces, it can transfer energy to nearby fluorophores through BRET, causing them to emit light. Adapted from Zambito 2021 [1].

Most BRET-activated nanoparticle designs like these are more commonly being used for *in vivo* phototherapy or tumor targeting applications and less for imaging and tracking *in vivo* [36,37]. Furthermore, there has been little research done on directly immobilizing BRET-based fusion reporters onto nanoparticles for BLI. BRET-based reporters on nanoparticles could produce more efficient BRET-based luminescence than using separate luminescent and fluorescent molecules like current designs. Thus, in this study, we explored the potential of assembling BRET-based reporters onto the E2 nanoparticle for improved BLI.

1.5. BRET-based reporter conjugated E2 nanoparticle as an enhanced bioimaging reporter

Based on previous work described above that highlighted the improved luminescence output of Nluc when conjugated to a nanoparticle, **we hypothesized that BRET-based reporters immobilized onto a nanoparticle could produce an enhanced light output**

compared to free BRET-based reporters. By being immobilized on a nanoparticle, the luciferase in the fusion reporter could experience a greater catalytic efficiency and thus produce a greater light output. This would result in more light energy being available to excite the fluorophore through BRET and a greater BRET efficiency could result in a greater light signal. **We also hypothesized that we could develop luminescent nanoparticles that were more red-shifted than Nluc-E2 by choosing a BRET-based fusion reporter with a red-shifted emission.** This strategy of BRET-based reporter conjugated nanoparticles could enable more sensitive *in vivo* BLI.

In this thesis work, we immobilized two different BRET-based reporters, CeNLuc and LumiScarlet, onto the E2 nanoparticle platform to investigate the potential for BRET-based reporter conjugated nanoparticles (CeNLuc-E2 and LumiScarlet-E2) as enhanced imaging platforms. E2 is a protein assembly derived from the pyruvate dehydrogenase complex of *Geobacillus stearothermophilus* that self-associates into a dodecahedral cage consisting of 60 identical subunits [38]. The E2 protein complex is approximately 24-nm in diameter and can be engineered at the internal, external, and inter-subunit interfaces [39]. E2 has been recombinantly fused to SpyTag (ST) yielding ST-E2, to enable the conjugation of SpyCatcher-fused proteins to the surface of ST-E2 through the SpyCatcher-SpyTag interaction [28]. Thus, CeNLuc and LumiScarlet were recombinantly fused to SpyCatcher (SC), yielding SC-CeNLuc and SC-LumiScarlet, for conjugation to ST-E2 (Figure 4b).

CeNLuc and LumiScarlet were chosen for immobilization because they exhibit optimal imaging properties such as an intense light output or a red-shifted emission [12,26]. CeNLuc comprises a cyan fluorescent protein, mCerulean3, fused to NLuc with a flexible five amino acid linker in between (Figure 4a). The mCerulean3 protein was chosen as the BRET acceptor

because it has a high quantum yield, photostability, and pH insensitivity [40]. Furthermore, the BRET pair demonstrates high BRET efficiency, as the NLuc emission has a high spectral overlap with the mCerulean3 excitation spectrum [26]. The emission of CeNLuc is centered at 475 nm and when expressed in cells, CeNLuc showed about 4-fold brighter total light output than Nluc [26]. Thus, we hypothesized that if we conjugated CeNLuc onto E2, we could produce a brighter and less blue-shifted luminescent nanoparticle than Nluc-E2.
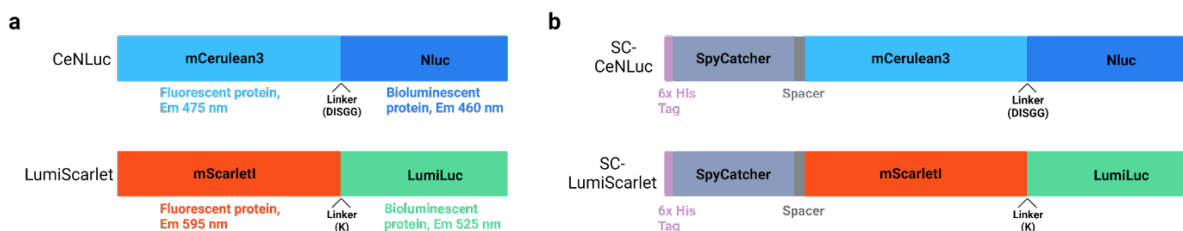
Figure 4. CeNLuc and LumiScarlet constructs. a) Original genetic constructs [12,26]. b) Constructs fused to SpyCatcher used in this study.

LumiScarlet was chosen as the other reporter to immobilize to E2 because LumiScarlet exhibits a red-shifted emission around 595 nm [12]. LumiScarlet is a fusion of the mScarletI fluorescent protein with LumiLuc (Figure 4a). The mScarletI protein was selected as the BRET acceptor because it is red-shifted, has a high quantum yield and has previously exhibited good performance as an energy acceptor [41]. LumiLuc was chosen as the luciferase donor because its emission, centered around 525 nm, has a greater spectral overlap with the excitation spectrum of mScarletI, making it a more efficient donor for BRET than Nluc [12]. Furthermore, LumiLuc catalyzes 8pyDTZ substrate, which exhibits high solubility and could be administered at higher doses *in vivo* than conventional substrates [12]. Approximately half of the LumiScarlet emission was found to be longer than 600 nm [12]. In an *in vivo* study, LumiScarlet showed about 3-fold higher signals than LumiLuc, demonstrating LumiScarlet's capacity as a more sensitive reporter

for deep tissue imaging [12]. We hypothesized that immobilizing LumiScarlet onto E2 would enable a more sensitive reporter with enhanced tissue penetration properties.

1.6. Objectives

The aim of this thesis is to explore the assembly of BRET-based reporters onto the E2 nanoparticle platform to produce brighter, more red-shifted luminescent reporters. This BRET-based luminescent nanoparticle platform could enable improved BLI for broad *in vivo* applications such as tumor tracking or biodistribution studies. Specific objectives are listed as follows:

1. Genetically fuse CeNLuc and LumiScarlet genetic constructs to SpyCatcher and express and purify SpyCatcher recombinant proteins

2. Conjugate BRET-based recombinant proteins, SC-CeNLuc and SC-LumiScarlet, onto SpyTag-E2 (ST-E2) nanoparticles and assess different ratios of luminescent proteins to a nanoparticle and its effect on luminescence

3. Assess if the luminescent emission produced by CeNLuc-E2 and LumiScarlet-E2 is resultant from BRET

4. Evaluate the luminescence of CeNLuc-E2 and LumiScarlet-E2 nanoparticles in comparison to free CeNLuc and free LumiScarlet *in vitro*

5. Evaluate the red-shifted emission of BRET-activated nanoparticles to assess deep tissue imaging capacity

2. MATERIALS AND METHODS

2.1. Materials

All reagents were purchased from Fisher Scientific unless otherwise noted. BRET-based reporter plasmids were received from Addgene (CeNLuc: cat. no. #135934 and LumiScarlet: cat. no. #126623). Restriction endonucleases were purchased from New England Biolabs. DNA oligonucleotides were purchased from Integrated DNA Technologies. The GeneJET Gel Extraction Kit and Micro BCA Protein Assay Kit were from Thermo Scientific. The QIAprep Spin Miniprep Kit was from Qiagen. The Nano-Glo™ Luciferase Assay System (N1120) was purchased from Promega. The 8pyDTZ (HY-135368) was purchased from MedChemExpress.

2.2. Cloning of constructs and genetic fusion of constructs to SpyCatcher

Plasmids for CeNLuc and LumiScarlet were from Addgene and the plasmid maps can be found in Appendix A. For constructs that were to be ligated to SpyCatcher (SC-CeNLuc, SC-mCerulean3, SC-LumiScarlet, SC-mScarletI, and SC-LumiLuc), forward primers were designed with a N-terminal *Nhe*I site plus a spacer. For the non-SpyCatcher constructs (CeNLuc, mCerulean3, LumiScarlet, mScarletI, LumiLuc), primers with a N-terminal *Nhe*I site and 6X-His tag were encoded. Lastly, reverse primers were encoded with a C-terminal *Bam*HI site for all constructs. All primers used are listed in Appendix B. The genes of interest were amplified through polymerase chain reaction (PCR) using standard PCR protocol [42]. The amplified genes were then ligated to the pJET1.2 blunt vector. The vectors were transformed into *E. coli* (DH5α) cells and the DNA was purified using the Qiagen miniprep kit. The genetic constructs were sequenced with Sanger's sequencing from GeneWiz Azenta and confirmed. Plasmid maps, DNA sequences, and amino acid sequences of the constructs are presented in Appendix C-E. The genes and vectors of interest were then digested with *Nhe*I and *Bam*HI and extracted from 0.8%

agarose gels using the GeneJET purification kit. The constructs to be fused to SpyCatcher were ligated overnight to a pET11a-SpyCatcher vector and non-SpyCatcher constructs were ligated overnight to pET11a (Appendix C). The pET11a ligations were transformed into DH5α cells, minipreps of the plasmids were made, and a check digest agarose gel was run to confirm the genes were ligated to the vector. The confirmed purified plasmids were transformed into chemically competent BL21 (DE3) cells for expression.

2.3. Expression, purification and characterization of luminescent proteins

Small-scale expressions were performed initially to determine the optimal expression conditions for each protein. Colonies were inoculated into 5 mL LB cultures with 100 μg/ml ampicillin and incubated overnight at 37°C for 16 hours. The overnight cultures were then inoculated into fresh 5 mL LB cultures containing 100 μg/ml ampicillin and incubated until the OD_{600} reached 0.6-0.9 [28]. From there, the induction and expression steps were done using variable conditions for the CeNLuc and LumiScarlet proteins.

CeNLuc and its SC-fusion proteins were induced with 1mM IPTG and expressed at 37°C for 3 hours or at 20°C for 16 hours. Cells were then harvested, resuspended in Tris buffer, and frozen at -80°C. Cells were lysed using glass beads and the soluble fraction was separated from the insoluble fraction and both fractions were run on SDS-PAGE gels. More soluble proteins were observed for proteins expressed at 20°C for 16 hours, and this was the expression condition used for the large-scale expression of all proteins, except SC-CeNLuc, which was further optimized (Figure S1). SC-CeNLuc was expressed at 20°C for 16 hours and at 16°C for 24 hours with final concentrations of IPTG at 1, 0.5, 0.1, and 0.05 mM IPTG. SDS-PAGE of the cell lysates showed higher soluble protein fractions for proteins expressed at 16°C with 0.1 or 0.05 mM IPTG. The final expression condition for SC-CeNLuc was 16°C with 0.1 mM IPTG.

For LumiScarlet and its SC-fusion proteins, the initial induction and expression conditions used were 20°C for 16 hours with 1 mM IPTG. SDS-PAGE of the soluble and insoluble fractions showed that all proteins expressed half or more proteins in the soluble fraction, except SC-LumiScarlet, which was further optimized. SC-LumiScarlet was expressed at 20°C for 16 hours and at 16°C for 24 hours using 1 and 0.1 mM IPTG. Proteins expressed at 20°C with 0.1 mM IPTG showed more soluble protein expression and was the final expression condition used (Figure S2).

For the final expression, colonies were inoculated into 5 mL LB cultures supplemented with ampicillin and incubated overnight at 37°C for 16-18 hours. Overnight cultures were inoculated into 200 mL cultures containing ampicillin and incubated until the OD_{600} reached 0.6-0.8. Cultures were then induced at the conditions optimal to each protein. Cells were harvested and pellets were frozen at -80°C. Next, cells were broken and the proteins were purified. Cells were resuspended in breaking buffer, 1mM PMSF was added, and cells were lysed using a french press. 1X HALT protease inhibitor was added to the lysate to further prevent any protein degradation. The cell lysate was spun in the Optima™ XPN-80 ultracentrifuge (Beckman Coulter) using the Type 45 Ti Rotor and at a speed of 35,000 xg to separate the soluble fraction from the insoluble fraction. The soluble fraction was purified using the HisPur Ni-NTA affinity columns. Columns were washed with imidazole at a range of concentrations (25, 50, 100, 150, 200, 250 mM imidazole). Samples from all elution steps were run on SDS-PAGE and fractions containing the protein were pooled together. The purified proteins were buffer exchanged in phosphate-buffered saline (PBS) (137 mM NaCl, 2.7 mM KCl, 10mM Na_2HPO_4, 1.8 mM KH_2PO_4) to remove the imidazole and then concentrated using an amicon filter. Purified proteins were aliquoted and stored at -80°C.

The final proteins were characterized for purity and molecular weight through

SDS-PAGE (Figure S3). Protein concentrations were measured with the Micro BCA protein

assay. However, LumiScarlet, SC-LumiScarlet, mScarlet, and SC-mScarlet protein

concentrations were measured using gel quantification with ImageJ because their absorbance

(Abs 569 nm) overlapped with absorbance of the BCA (Abs 562 nm). Concentrations of proteins

measured with BCA were also confirmed using gel quantification. Nluc, SC-Nluc, and ST-E2

were previously purified and characterized in the lab and stored in the -80°C [28].

2.4. Spectral characterizations of luminescent proteins and luminescent nanoparticles

The fluorescent spectra of proteins were measured using the SpectraMax M2 microplate

reader (Molecular Devices, LLC). Emission spectra were measured from 440-600 nm using 5 nm

increments and an excitation of 433 nm for proteins containing mCerulean3. Proteins containing

mScarletI, were measured from 580 to 650 nm with an excitation of 569 nm. For fluorescent

measurements 100 ul of protein were added to 96-well black opaque plates (Greiner). The final

concentration of proteins containing mCerulean3 was 3 μM and of proteins containing mScarletI

was 10 μM. Samples were diluted in phosphate buffer (50mM KH_2PO_4, 100mM NaCl) at pH 7.4,

which also served as the background sample.

Luminescence spectra of the luminescent proteins and luminescent particles were

measured using the SpectraMax M3 microplate reader (Molecular Devices, LLC). Protein or

nanoparticle samples of 50 ul were added to 96-well, white, clear bottom plates (Thermo

Scientific). Right before the measurement, 50 μl of substrate was added to wells. The final

concentration of the luminescent proteins and luminescent nanoparticles was 5 nM of luciferase.

For proteins with Nluc a 1:50 dilution of furimazine (Nano-Glo® Luciferase Assay System,

Promega) was used as the substrate. For proteins with LumiLuc, 8pyDTZ (MedChem Express) at

14

a final concentration of 100 uM was used as the substrate. For samples with Nluc, spectra were

measured from 400-600 nm and for samples with LumiLuc spectra were measured from 400-700

nm. Measurements were made in 5 nm increments with 250 ms integration time. Samples were

diluted in phosphate buffer. Phosphate buffer with substrate served as the background sample.

2.5. Conjugation of luminescent proteins to ST-E2 and luminescence of luminescent-E2 particles

To synthesize the luminescent-E2 particles, the SC-luminescent proteins and ST-E2 were

mixed together at specific molar ratios of luminescent protein to ST-E2 monomer. The

components were mixed in phosphate buffer (50mM KH_2PO_4, 100mM NaCl) at pH 7.4 and

allowed to react at room temperature for 2 hours on a shaker, followed by incubation at 4°C

overnight. The conjugation reactions were spun down at 18,000 xg for 10 minutes to separate out

any insoluble fraction.

Dynamic light scattering (DLS) (Malvern Zetasizer, Nano ZS) was performed on the

conjugations to determine the hydrodynamic diameter and monodispersity of the particles. The

conjugation ratio of luminescent proteins to ST-E2 subunits was quantified based on

densitometry of SDS-PAGE gels measured using ImageJ. Concentrations of the conjugated

particles were determined using the BCA protein assay.

SC-CeNLuc was conjugated to ST-E2 particles at varying molar ratios (0.7:1, 0.5:1,

0.35:1, 0.25:1, 0.1:1) of SC-CeNLuc to ST-E2 monomer. Different molar ratios were used to

determine the maximum number of luminescent proteins that could be immobilized without the

presence of excess unconjugated proteins. Luminescence of CeNLuc-E2 particles of varying

molar ratios was measured using the SpectraMax M3 microplate reader. Sample titrations were

made for final in-well concentrations of 15, 7.5, and 3.75 nM of Nluc and 50 ul of sample was

added to 96-well white, clear bottom plates (Thermo Scientific). Before taking the measurement, 50 ul of a 1:50 dilution of FRZ was added to the samples. Phosphate buffer with FRZ served as the background. Samples were run in duplicates and total luminescence was measured.

2.6. *In vitro* luminescence assays

Luminescence of the monomeric proteins and nanoparticle samples was measured using the IVIS Lumina CCD camera (PerkinElmer). The CCD camera was chilled to -83°C and the imaging stage was kept at 37°C during the imaging. The excitation was set to block and emission set to open. For red-shifted measurements the emission filter was set to DsRed. Exposure time ranged from 0.5 to 2 s, binning was set to medium, field of view was 12.5 cm, and f number was set to 1. Protein samples were loaded into 96-well black, clear bottom plates (Corning). The sample volume was 50 ul and the final concentration was 10 nM of luciferase. Before imaging, a 1:50 dilution of furimazine in phosphate buffer (50mM KH_2PO_4, 100mM NaCl) was added to samples containing Nluc. For samples containing LumiLuc, 50 ul of 8pyDTZ with a final concentration of 100uM was added. For the background measurement, 50 ul of substrate was added to 50 ul of phosphate buffer. The final in-well volume of all samples was 100 ul. Living Image Software version 4.1.3 was utilized to select regions of interest after imaging to quantify the total flux.

2.7. Statistical analysis

The statistical analyses were performed using GraphPad Prism. We utilized one-way ANOVA with Tukey's multiple comparison test over the experimental groups. Data were represented as mean ± standard error of mean (SEM) for all experiments and n=3 for experiments, unless stated otherwise. In all cases, $p < 0.05$ is considered statistically significant.

3. RESULTS AND DISCUSSION

3.1. CeNLuc and LumiScarlet constructs fused to SpyCatcher maintained their spectral properties

CeNLuc and LumiScarlet were chosen as the BRET–based reporters for immobilization to SpyTag-E2. To conjugate the proteins onto ST-E2 using the SpyCatcher-SpyTag conjugation [43,44], recombinant luminescent proteins were made by fusing SpyCatcher (SC) to the N-terminus of CeNLuc and LumiScarlet, yielding SC-CeNLuc and SC-LumiScarlet. SpyCatcher fusions were also made for the individual bioluminescent and fluorescent proteins that comprised the BRET-based fusion constructs, yielding SC-mCerulean3, SC-mScarletI, and SC-LumiLuc.
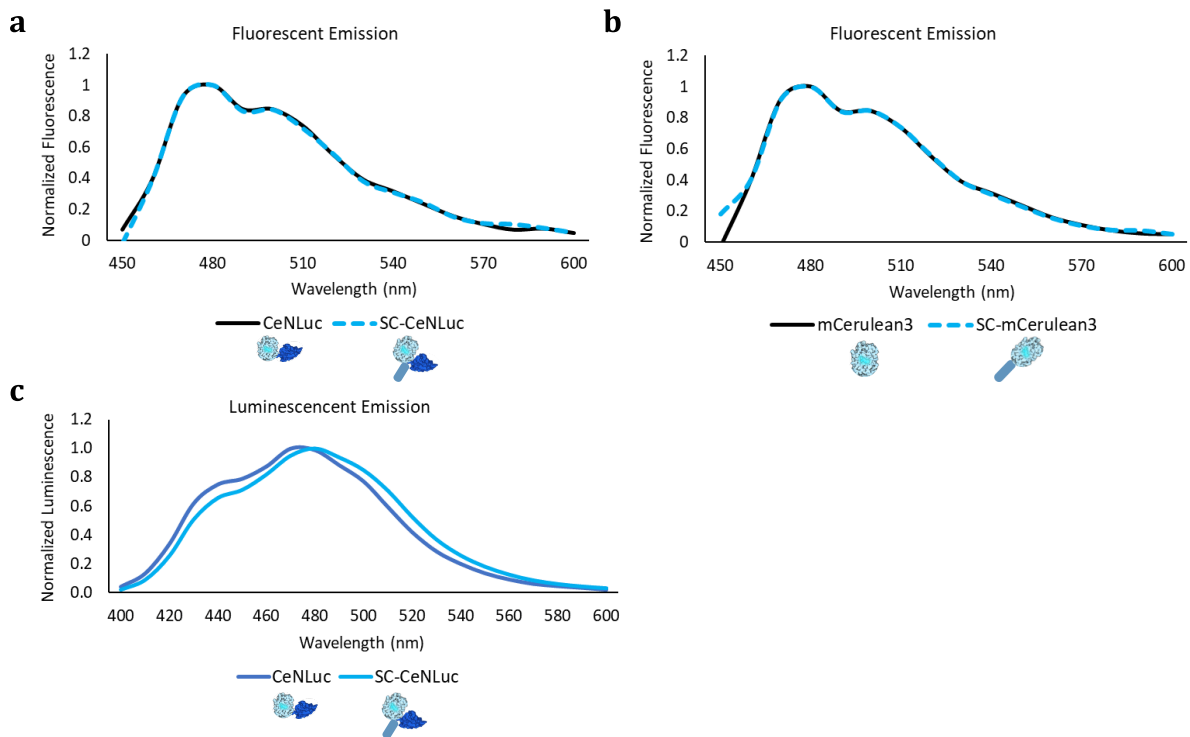

Figure 5. Spectral characterizations of CeNluc, SC-CeNLuc, mCerulean3, and SC-mCerulean3. a,b) The fluorescent emission maximum for CeNLuc, SC-CeNLuc, mCerulean3, and SC-mCerulean3 was at 475 nm. c) The luminescent emission of CeNLuc and SC-CeNLuc was centered at 475 nm. Data was normalized to the emission maximum of each peak. Spectra were measured in duplicates and representative images are shown.

All SC-fusion proteins were successfully expressed and purified. In addition to the SC-fusion proteins, non-SC proteins for all BRET, fluorescent, and bioluminescent proteins were purified as well (CeNLuc, LumiScarlet, mCerulean3, mScarletI, LumiLuc). All the luminescent proteins used in this study are summarized in Table 1. Final purified proteins were run on SDS-PAGE and their molecular weights were confirmed (Figure S3, Table 1). Fluorescent and luminescent spectral characterizations were also performed to confirm that fusion to SC did not affect the spectral signature of the proteins (Figure 5, 6). There was no change to the emission profiles or to the emission wavelengths of the SC-proteins compared to the non-SC proteins.
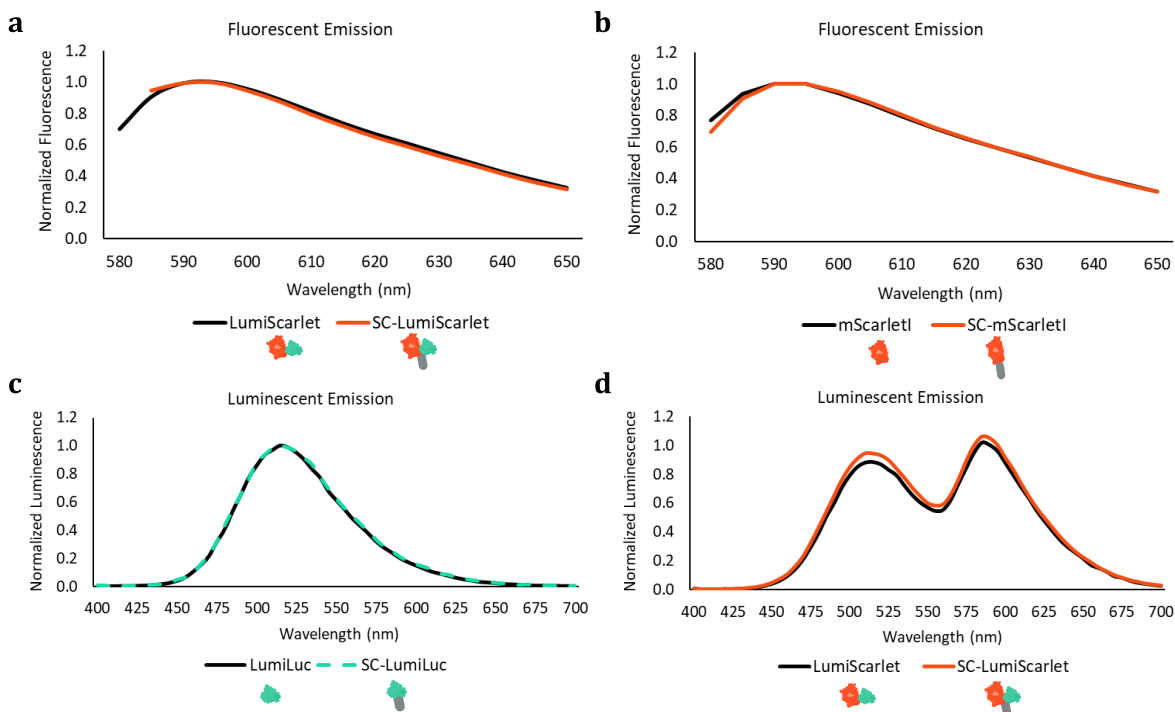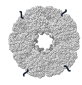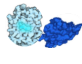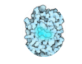

Figure 6. Spectral characterizations of mScarletI, SC-mScarletI, LumiScarlet, SC-LumiScarlet, LumiLuc, and SC-LumiLuc. a,b) The fluorescent emission peak for mScarletI, SC-mScarletI, LumiScarlet, SC-LumiScarlet was at 595 nm. c) For LumiLuc and SC-LumiLuc, the bioluminescent emission was at 515 nm. d) The luminescent emission of LumiScarlet and SC-LumiScarlet displayed a bimodal spectrum, with an emission peak at 595 nm and a second peak at 515 nm. Data was normalized to the emission maximum of each peak. Measurements were performed in triplicates and representative images are shown.

Table 1. Descriptions of proteins used in this study

Protein	Molecular Weight (kDa)	Representation	Description
ST-E2	30.3 (monomer)		Assembly of 60 ST-E2 monomers; SpyTag fused onto the N-terminus of E2 (D381C)
CeNLuc	46.9		BRET-fusion of mCerulean3 fused to N-terminus of Nluc
SC-CeNLuc	62.2		SC fused to N-terminus of CeNLuc
mCerulean3	27.3		Cerulean blue fluorescent protein
SC-mCerulean3	42.7		SC fused to N-terminus of mCerulean3
Nluc	19.9		NanoLuc luciferase
SC-Nluc	35.1		SC fused to N-terminus of Nluc
LumiScarlet	45.1		BRET-fusion of mScarletI fused to N-terminus of LumiLuc
SC-LumiScarlet	60.3		SC fused to N-terminus of LumiScarlet
mScarletI	26.3		Scarlet red fluorescent protein
SC-mScarletI	41.5		SC fused to N-terminus of mScarletI
LumiLuc	19.6		LumiLuc luciferase
SC-LumiLuc	34.8		SC fused to N-terminus of LumiLuc

3.2. Conjugation of CeNLuc and LumiScarlet onto E2 resulted in monodisperse CeNLuc-E2 and LumiScarlet-E2 nanoparticles of approximately 35-nm in size

SC-CeNLuc and SC-LumiScarlet were conjugated to ST-E2 using the SC-ST approach [43,44]. A pilot study was run to determine the optimal ratio of BRET-based protein to ST-E2 monomer that would result in the complete conjugation of the luminescent proteins without any unconjugated proteins present. SC-CeNLuc was conjugated to ST-E2 at molar ratios of 0.7, 0.5, and 0.25 moles of SC-CeNLuc to 1 mole of ST-E2 subunit, resulting in CeNLuc-E2 nanoparticles with varying amounts of luminescent proteins conjugated to the exterior of E2. SDS-PAGE showed that the CeNLuc-E2 monomers were at the expected molecular weights of 91 kDa (Figure S4). However, the 0.7:1 and 0.5:1 molar ratio conditions showed excess unconjugated SC-CeNLuc, whereas the 0.25:1 molar ratio showed complete conjugation of SC-CeNLuc to ST-E2. The conjugation of CeNLuc to the nanoparticle maxed out around 30 SC-CeNLuc proteins per 1 ST-E2 nanoparticle. Although the ST-E2 nanoparticle is composed of 60 monomers, the conjugation of CeNLuc reached a maximum at half of the monomers conjugated. This could be due to the large size of the SC-CeNLuc proteins (~60 kDa) relative to the ST-E2 monomer (~30 kDa) resulting in steric hindrance and preventing more proteins from conjugating to the monomers.

It was decided that a molar ratio of less than 0.5:1 SC-CeNLuc to ST-E2 monomer would be ideal to use to eliminate the chance of unconjugated proteins being present in the conjugation reaction. Ratios lower than 0.5:1 were tested, which included 0.35:1 and 0.1:1. These conjugation ratios also resulted in complete conjugation of SC-CeNLuc to the nanoparticle. A luminescence assay was performed to assess whether the number of luminescent proteins conjugated to a nanoparticle would affect the luminescence of CeNLuc-E2 nanoparticles

containing equimolar amounts of Nluc. The luminescence of particles conjugated with 0.5:1, 0.35:1, and 0.25:1 moles of SC-CeNLuc to ST-E2 was measured after the addition of furimazine substrate. No significant difference was observed in luminescence, whether particles had more or less CeNLuc immobilized on the surface (Figure 7). CeNLuc-E2 with a conjugation ratio of 0.25:1 was chosen for subsequent studies. Each CeNLuc-E2 nanoparticle had 12.8 ± 0.6 CeNLuc proteins conjugated to its surface (Table 2, construct 2). CeNLuc-E2 was measured to be 36.3 ± 1.5 nm in diameter, slightly larger than ST-E2 particles which were found to be 29.3 ± 0.3 nm (Table 2, construct 1), indicating conjugation of CeNLuc to the E2 surface.
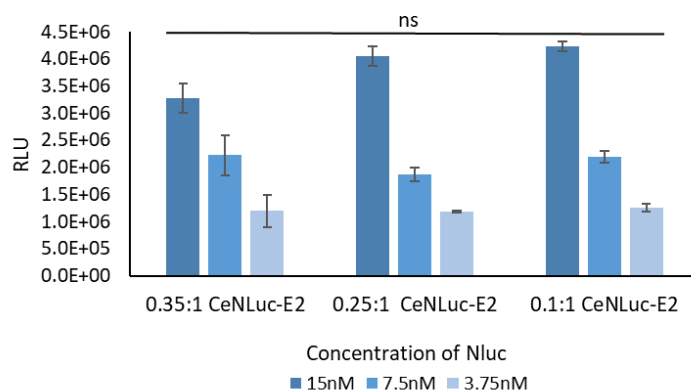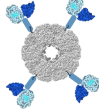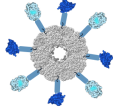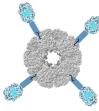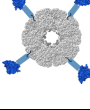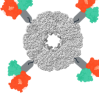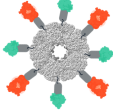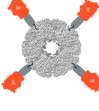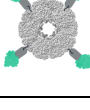
Figure 7. Mean luminescence of different conjugation ratios of SC-CeNLuc to ST-E2. Molar ratios of 0.35:1, 0.25:1, and 0.1:1 CeNLuc to E2 monomer were tested. Samples contained equimolar concentrations of Nluc and FRZ was used as the substrate. Data are represented as mean $\pm$ SEM of n=3 independent experiments, with background (phosphate buffer+ FRZ) subtracted. One-way ANOVA with Tukey's multiple comparison test were performed and ns= no significance between the different ratios at a given Nluc concentration.

As mentioned earlier, most BRET-activated nanoparticle designs have not directly utilized BRET-based fusion reporters on nanoparticles [31,35,36]. Instead, they immobilize luciferases onto fluorescent particles or fluorophore loaded particles to produce BRET-based emission. We hypothesized that conjugation of BRET-fusion reporters on particles would produce more efficient BRET-based emission than separately conjugating luminescent and fluorescent proteins onto particles. This is due to the fact that the efficiency of BRET between

luciferase donors and fluorophore acceptors is high when both are within <10 nm of each other [14]. In addition to CeNLuc-E2 (Table 2, construct 2), we tested two additional nanoparticle designs to model BRET. The (mCerulean3+Nluc)-E2 nanoparticle (Table 2, construct 3) consists of nanoparticles conjugated with equimolar amounts of mCerulean3 fluorescent protein and Nluc protein on the surface. The other design comprised Nluc conjugated particles, Nluc-E2 (Table 2, construct 5), mixed with mCerulean3 conjugated nanoparticles, mCerulean3-E2 (Table 2, construct 4), at equimolar amounts of luminescent protein. Particles were conjugated with the same 0.25:1 molar ratio of protein to E2 subunit, so that equal ratios of fluorescent and bioluminescent proteins were conjugated to the nanoparticles in comparison to CeNLuc-E2.

Since the maximum conjugation of luminescent proteins to a nanoparticle was determined to be about 30 proteins, a higher molar conjugation ratio was not chosen for studies because a ratio higher than 0.25:1 would require more than 30 proteins for the (mCerulean3+Nluc)-E2 nanoparticle (Table 2, construct 3). With a 0.25:1 ratio, the (mCerulean3+Nluc)-E2 nanoparticle had about 14 fluorescent proteins and 14 bioluminescent proteins conjugated for a total of about 28 proteins conjugated to the nanoparticle (Table 2, construct 3). So although a slightly higher ratio such as 0.35:1 could have been used for CeNLuc-E2, it would have required more than 30 of the fluorescent and bioluminescent proteins to conjugate to E2 to observe the equivalent conjugation ratio, which could have resulted in excess unconjugated proteins for the (mCerulean3+Nluc)-E2 nanoparticle. Successful conjugations were observed for the (mCerulean3+Nluc)-E2 (Table 2, construct 3), mCerulean3-E2 (Table 2, construct 4), and Nluc-E2 (Table 2, construct 5) nanoparticles using the 0.25:1 molar conjugation ratio. Conjugations were confirmed to be at the expected molecular weights based on SDS-PAGE (Figure S5).

Table 2. Characterizations of luminescent nanoparticles

Construct	Representation	Conjugation Ratio (Moles Protein: Mole ST-E2 subunit)	Proteins per Nanoparticle (n=3)	Hydrodynamic Diameter (nm) (n=3)
#1 ST-E2		—	—	29.3 ± 0.3
#2 CeNLuc-E2		0.25 CeNLuc: 1	12.8 ± 0.6 CeNLuc	36.3 ± 1.5
#3 (mCerulean3 + Nluc)- E2		0.25 mCerulean3: 0.25 Nluc: 1	13.9 ± 1.0 mCer. 13.9 ± 0.3 Nluc	34.4 ± 0.5
#4 mCerulean3-E2		0.25 mCerulean3: 1	12.2 ± 0.8 mCer.	32.2 ± 0.5
#5 Nluc-E2		0.25 Nluc: 1	12.6 ± 0.2 Nluc	32.2 ± 0.5
#6 LumiScarlet-E2		0.25 LumiScarlet: 1	13.1 ± 1.6 LumiScarlet	35.0 ± 0.6
#7 (mScarletI + LumiLuc)-E2		0.25 mScarletI: 0.25 LumiLuc: 1	11.1 ± 2.0 mScar. 10.6 ± 1.4 LumiLuc	34.2 ± 1.2
#8 mScarletI-E2		0.25 mScarletI: 1	12.2 ± 2.1 mScar.	32.0 ± 0.2
#9 LumiLuc-E2		0.25 LumiLuc: 1	10.6 ± 2.5 LumiLuc	31.6 ± 0.7

The same conjugation ratio of 0.25:1 was used for LumiScarlet-E2 and the other LumiScarlet-based particles. LumiScarlet-E2 (Table 2, construct 6), (mScarletI+LumiLuc)-E2 (Table 2, construct 7), mScarletI-E2 (Table 2, construct 8), and LumiLuc-E2 (Table 2, construct 9) were successfully conjugated and their molecular weights were confirmed on SDS-PAGE (Figure S6). For each LumiScarlet-E2 nanoparticle, there were ~13 SC-LumiScarlet proteins conjugated. LumiScarlet-E2 was found to be 35-nm in size, comparable to the size of CeNLuc-E2 and slightly larger than ST-E2. Characterizations of size and the number of proteins conjugated per particle for all the particle constructs are listed in Table 2.

3.3. CeNLuc-E2 and LumiScarlet-E2 particles produced BRET-based luminescence

To evaluate whether BRET was occurring between the bioluminescent donors and fluorescent acceptors on the nanoparticles, spectral analysis of the nanoparticle emission profiles was performed (Figure 8). BRET between the donor and acceptor would result in an emission peak appearing at the emission of the fluorescent protein [45]. CeNLuc-E2 demonstrated an emission peak at 475 nm comparable to the emission maximum of mCerulean3, indicating that energy transfer occurred from Nluc to mCerulean3 (Figure 8a) [26]. Compared to Nluc-E2, which had an emission peak of 440 nm, the emission of CeNLuc-E2 was 35 nm less blue-shifted. This shift in emission could show some benefits over Nluc-E2 for *in vivo* imaging applications as more blue-shifted light is highly absorbed and scattered by tissue [25]. The other conditions, the (mCerulean3+Nluc)-E2 and mCerulean3-E2 + Nluc-E2 nanoparticles, produced emission peaks at 440 nm, with an emission profile comparable to Nluc-E2. This indicated that a majority of the light output of these particles was being produced from the Nluc and that there was little to no resonance energy transfer from Nluc to mCerulean3. The emission peak of (mCerulean3+Nluc)-E2 and mCerulean3-E2 + Nluc-E2 particles did exhibit a small shoulder

around 475 nm, which suggests that some BRET could have possibly occurred between some of the Nluc and mCerulean3 proteins on the particles (Figure 8a).
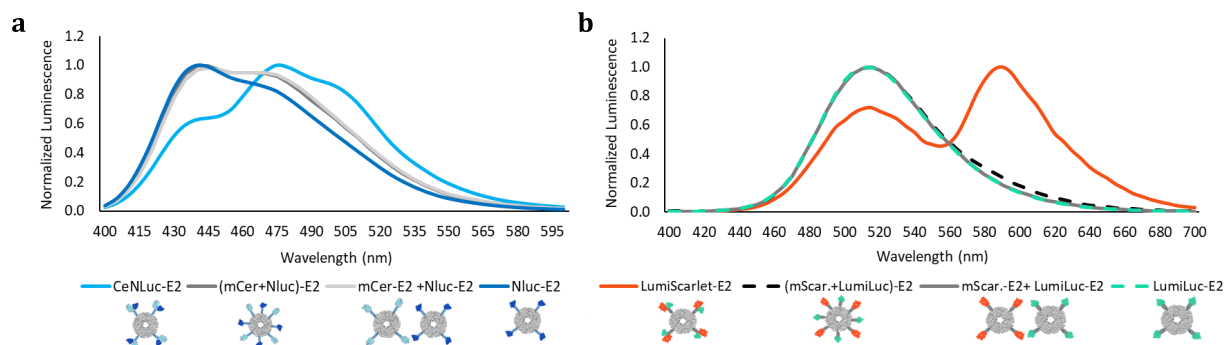
Figure 8. Luminescent spectral profiles of conjugated nanoparticles. a) Emission spectra of Nluc-based nanoparticles measured after the addition of FRZ. b) Emission spectra of LumiLuc-based particles after the addition of 8pyDTZ. Data is normalized to the emission maximum of each particle. Measurements were performed in triplicates and representative data are shown.

Assessing the emission of LumiScarlet-E2, the spectral profile displayed a bimodal spectrum with an emission peak at 595 nm and an additional smaller peak at 515 nm (Figure 8b). The LumiScarlet-E2 emission was 80 nm more red-shifted from the LumiLuc-E2 emission, which was centered at 515 nm. The LumiScarlet-E2 emission was produced by BRET from LumiLuc to mScarletI of the LumiScarlet fusion protein, as evidenced by the LumiScarlet-E2 emission (Em 595 nm) peaking at the emission of mScarletI (Em 595 nm). The other BRET-based particles, (mScarletI+LumiLuc)-E2 and mScarletI-E2 + LumiLuc-E2, exhibited emission peaks centered at 515 nm similar to LumiLuc-E2 (Figure 8b). Their emission profiles were also comparable to the LumiLuc-E2 profile. This indicated that these two conditions, with separately conjugated LumiLuc donors and mScarletI acceptors, were likely unable to undergo BRET as there was no other emission peak observed around 595 nm nor any shift in emission profile observed compared to LumiLuc-E2 (Figure 8b).
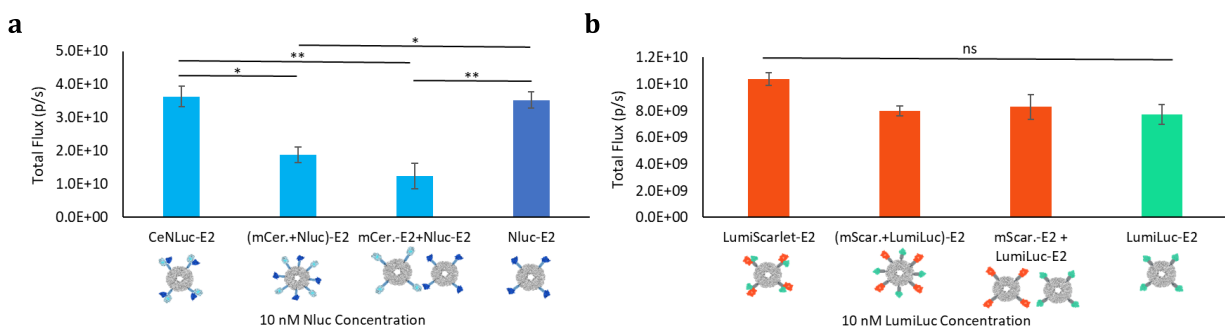
Figure 9. Luminescence using IVIS of BRET-based particle designs compared to bioluminescent, luciferase-only particles. a) Luminescence of BRET-based particles using Nluc as the BRET donor, measured after the addition of FRZ. b) Luminescence of BRET-based particles using LumiLuc as the BRET donor, measured after the addition of 8pyDTZ. All measurements were performed in triplicates and data are represented as mean ± SEM with background (phosphate buffer + substrate) subtracted. One-way ANOVA with Tukey's multiple comparison test were performed (*$p <0.05$, **$p <0.01$).

In addition to the spectral characterizations, the total luminescence intensity of all the BRET-modeling nanoparticles was also measured to compare the total light output of particles directly conjugated with BRET-fusion proteins versus particles conjugated with separate bioluminescent and fluorescent proteins. In luminescence assays of particle samples containing equimolar amounts of Nluc, the CeNLuc-E2 nanoparticles showed significantly greater total flux compared to the other two BRET-based nanoparticles (Figure 9a). CeNLuc-E2 exhibited at least 2-fold higher luminescence than the (mCerulean3+Nluc)-E2 and mCerulean3-E2 + Nluc-E2 particles (Figure 9a). Even if BRET didn't occur for the (mCerulean3+Nluc)-E2 and mCerulean3-E2 + Nluc-E2 particles, they were expected to produce luminescence at least comparable to Nluc-E2, as all the particle conditions contained equal concentrations of Nluc. However, the luminescence of these particle conditions was lower. Signal quenching could not be a possibility, as CeNLuc-E2 didn't exhibit a reduced signal. Comparing all the LumiLuc-containing nanoparticles, LumiScarlet-E2 exhibited a higher flux (Figure 9b). In

addition, the (mScarletI+LumiLuc)-E2 and mScarletI-E2 + LumiLuc-E2 particles produced comparable luminescence to LumiLuc-E2 (Figure 9b).

Analyzing all three BRET-based particle designs, only the particles conjugated with the BRET-fusion proteins were able to exhibit BRET-based luminescence. The lack of BRET observed for the (mCerulean3+Nluc)-E2 and (mScarletI+LumiLuc)-E2 particles could possibly be attributed to a majority of the SC-fluorescent proteins and SC-bioluminescent proteins being conjugated farther apart from each other on the particle. The conjugation is a random process thus the localization of the fluorescent and bioluminescent proteins relative to each other can not be controlled. As such, there could be less BRET pairs that are within <10 nm apart for efficient BRET to occur. A recent study provided a method to calculate the estimated distance between the chromophores of BRET-fusion pairs [21]. Based on this method, we estimate the chromophores of the BRET pairs in CeNLuc to be ~4.2 nm apart and in LumiScarlet to be ~3.9 nm apart. Thus, if the fluorophore and luciferase are separately conjugated to E2, they are expected to be farther apart than when fused together.

We used the protein structures of E2, SpyCatcher, the fluorescent proteins, and the bioluminescent proteins to estimate the relative distances of the luminescent proteins when conjugated to E2. The E2 dodecahedron assembly comprises 20 trimers, so the closest conjugated E2 monomers would be located on the same trimer [46]. The (mCerulean3+Nluc)-E2 and (mScarletI+LumiLuc)-E2 particles were conjugated with an estimated 25 total fluorescent and bioluminescent proteins, which would suggest that if at least one luminescent protein conjugated to each trimer, there would be 5 trimers that could contain both a fluorescent and bioluminescent protein. We estimated that the closest distance between the SCs on a trimer would be around 3 nm where SC binds to ST (Figure S7). The SC-fluorescent protein and

SC-luminescent are expected to conjugate to ST-E2 at an outwards angle, so we estimated that the chromophores of the fluorescent protein and bioluminescent protein would be at least 5 nm apart (Figure S7). This would suggest that the small proportion of proteins that did conjugate on the same trimer, could potentially undergo BRET, yet it didn't seem to be observed. Assessing the distance between SCs on monomers of different trimers, the closest distance on neighboring trimers was estimated to be around 6 to 8 nm, thus the luminescent proteins conjugated would be even farther apart. The efficiency of energy transfer is known to sharply decrease as the distance between the BRET pairs increases. Since the SC-fluorescent protein and SC-bioluminescent protein were estimated to be more spatially separated than the BRET-fusions there is a reduced chance of them producing BRET-based emission. The specific BRET working distances of CeNLuc and LumiScarlet that produce the most efficient energy transfer have not been characterized, so it could be possible that larger separation distances result in little to no energy transfer for CeNLuc and LumiScarlet [21]. In addition to their spatial separation, the relative angular orientation of the electromagnetic dipoles of the acceptor and donor affects the efficiency of BRET [47,48]. As the fluorescent and bioluminescent proteins are fused to SC they could also be sterically hindered from optimally orienting relative to each other to induce efficient energy transfer while in proximity to each other, resulting in little to no BRET [47].

Similarly, for the BRET-based particle design that comprised bioluminescent-only particles mixed with fluorescent-only particles, even fewer proteins, approximately 10-12, were conjugated to individual particles (Table 2). As a result, the proteins on the mCerulean3-E2, Nluc-E2, mScarletI-E2, and LumiLuc-E2 particles would have a greater chance of assembling more dispersed around the particle. For BRET to occur between the mixed particles, specifically mCerulean3-E2 + Nluc-E2 and mScarletI-E2 + LumiLuc-E2, the luciferases on the

bioluminescent particle would have to come in close proximity to the fluorophores on the fluorescent particle. We predicted the likelihood of this interaction occurring would be lower than when the luciferase and fluorophore are fused together or on the same particle.

3.4. CeNLuc-E2 produced approximately 12-fold greater luminescence than unconjugated CeNLuc and produced a light output comparable to Nluc-E2

Next, we assessed whether immobilizing BRET-based reporters to the E2 nanoparticle enhanced their luminescent performance compared to reporters that were not immobilized. The luminescence of CeNLuc-E2, Nluc-E2, and the free luminescent proteins was observed under IVIS upon addition of furimazine (Figure 10a-b). All samples contained equimolar amounts of Nluc conjugated or unconjugated. Immobilizing CeNLuc onto E2 resulted in an enhancement of CeNLuc luminescence. Moreover, the luminescence of free SC-CeNLuc was lower than free CeNLuc, yet when it was conjugated to ST-E2 it produced a light output significantly greater than either of the free proteins. CeNLuc-E2 luminescence was approximately 12-fold greater than CeNLuc and ~18-fold greater than SC-CeNLuc (Figure 10a). The lower light output of SC-CeNLuc versus CeNLuc could be due to the fusion of SC to the fluorescent protein preventing it from folding in the most optimal conformation for efficient light production. The mCerulean3 protein forms a barrel structure with an intrinsic chromophore [40]. The first 10 amino acids of the N-terminal region are not involved in the barrel formation [49]. However, this segment has shown to be an integral part of one end of the protein and is thought to be essential in folding and in protecting the chromophore [49]. Although extensions to the N-terminus should not affect the barrel formation, modifications to the protein could result in the loss of fluorescence intensity [49], which could explain why SC-CeNLuc exhibits a lower light output than CeNLuc.
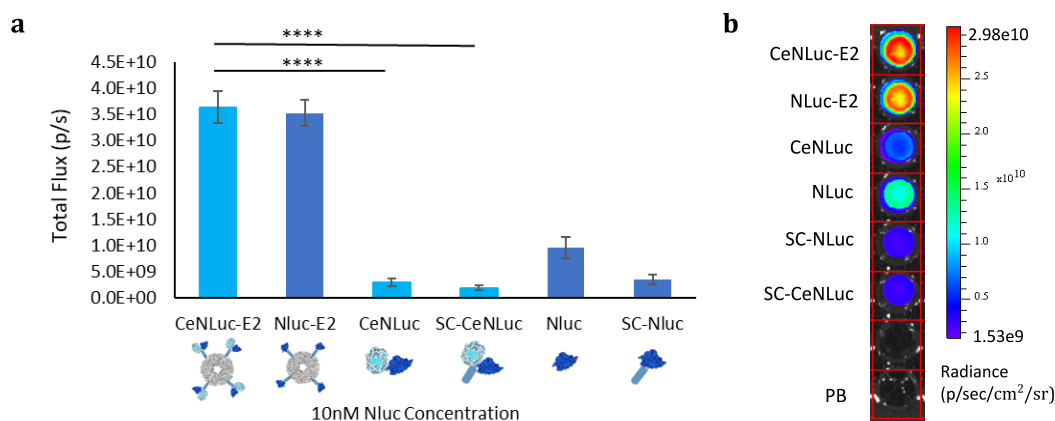
Figure 10. Total luminescence of conjugated versus unconjugated CeNLuc using IVIS. a) Luminescence of CeNLuc-E2, Nluc-E2, and the unconjugated luminescent proteins right after the addition of FRZ. Data are represented as mean ± SEM of n=3 independent experiments with background (phosphate buffer + FRZ) subtracted. One-way ANOVA with Tukey's multiple comparison test were performed (****p <0.0001). b) IVIS luminescence imaging of representative CeNLuc-E2 and Nluc-E2 particles along with unconjugated luminescent proteins after addition of FRZ.

When comparing the luminescence intensity of CeNLuc-E2 to Nluc-E2, no significant difference was observed (Figure 10a). We hypothesized that CeNLuc-E2 would be brighter than Nluc-E2 based on a previous study that showed CeNLuc was ~4-fold brighter than Nluc at equimolar concentrations [26]. However, in our studies we observed that CeNLuc luminescence was ~3-fold lower than Nluc (Figure 10a). One explanation for this difference could be that the previous study observed the luminescence of CeNLuc and Nluc proteins expressed in transiently transfected mammalian cells [26], whereas all our luminescence assays were performed with proteins expressed and purified from *E. coli*. The difference in microenvironment of the luciferase in cells versus in buffer could affect the luminescence output of the luciferase. Studies have shown that the polarity and even pH of the microenvironment can alter the binding interactions between luciferins and luciferases, affecting their emission properties [7,50]. Microenvironment changes would also affect the efficiency of the BRET interaction between the

luciferase and fluorescent protein because the luciferase activity is altered [50,51]. Based on the luminescence emission spectra of CeNLuc and SC-CeNLuc, it was evident that BRET transfer was occurring between the Nluc and mCerulean3 because the emission peak was centered around the emission of mCerulean3 (475 nm) (Figure 5c). The lower total intensity of CeNLuc could be due to a lower emission of Nluc in the CeNLuc fusion protein, affecting the efficiency of energy transfer from Nluc to mCerulean3. Although SC-CeNLuc luminescence was about 2-fold lower than SC-Nluc, when conjugated to the E2 nanoparticle, the luminescence of CeNLuc-E2 was comparable to Nluc-E2 (Figure 10a). Immobilizing CeNLuc onto E2 did not result in a luminescent reporter that was brighter than Nluc-E2. One advantage however was that the emission of CeNLuc-E2 was 35 nm less blue-shifted than Nluc-E2 and could exhibit a better tissue penetration depth than Nluc-E2 (Figure 8a). Yet, the emission of CeNLuc-E2 was still in the range of blue emission so a red-shifted luminescent nanoparticle was investigated next.

3.5. LumiScarlet conjugated to E2 (LumiScarlet-E2) retained its bioluminescence

To address the challenge of reduced signal sensitivity from luciferases *in vivo*, we looked at immobilizing a red-shifted BRET-based reporter, LumiScarlet, onto E2 as red-shifted emission displays enhanced deep tissue penetration. The luciferase in LumiScarlet is LumiLuc, which is an evolved version of Nluc that has been optimized for a substrate named 8pyDTZ to produce more red-shifted light than Nluc. LumiScarlet and LumiLuc were conjugated onto E2 to assay the luminescence intensity of LumiScarlet-E2 and LumiLuc-E2 in comparison to the unconjugated luminescent proteins after addition of 8pyDTZ (Figure 11). LumiScarlet-E2 produced luminescence comparable to free LumiScarlet and SC-LumiScarlet, suggesting that conjugation onto the nanoparticle assembly did not improve the luminescence of LumiScarlet (Figure 11a-b). LumiLuc-E2 also performed comparably to LumiScarlet-E2 and did not show

increased luminescence compared to unconjugated LumiLuc or SC-LumiLuc (Figure 11a). This trend was unlike what was observed for CeNLuc-E2 and Nluc-E2 and suggests that immobilizing LumiLuc or LumiScarlet onto E2 did not enhance the light output of the luciferase.
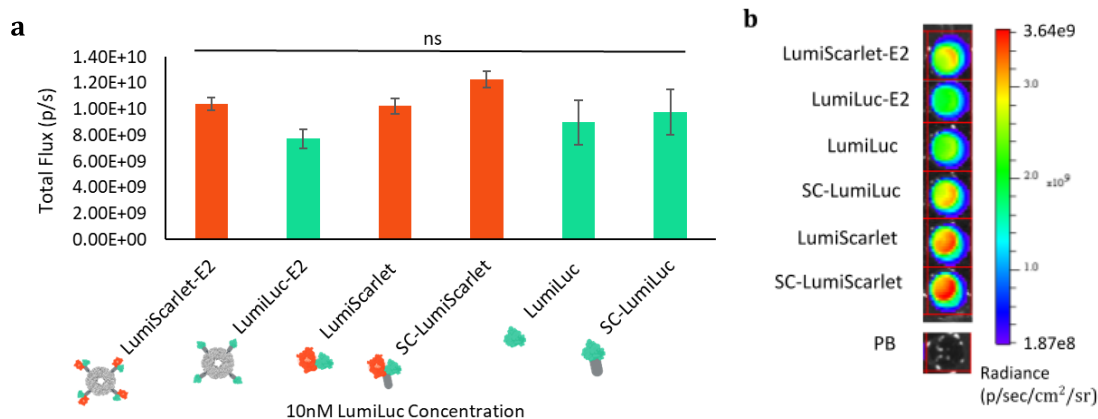
Figure 11. Total luminescence of conjugated versus unconjugated LumiScarlet and LumiLuc using IVIS. a) Luminescence of LumiScarlet-E2, LumiLuc-E2, and unconjugated luminescent proteins right after the addition of 8pyDTZ substrate. Data are represented as mean ± SEM of n=3 independent experiments with background (phosphate buffer + 8pyDTZ) subtracted. One-way ANOVA with Tukey's multiple comparison test were performed. b) IVIS luminescence imaging of representative LumiScarlet-E2 and LumiLuc-E2 particles along with unconjugated luminescent proteins after addition of 8pyDTZ.

Analyzing the protein structure of LumiLuc, the substrate binding site of the luciferase is comparable to the binding site of Nluc [12]. It faces outwards and away from the N-terminus of the protein where the SpyCatcher protein is fused. This suggests that the binding site of SC-LumiLuc and SC-LumiScarlet, when conjugated to ST-E2, should be oriented outward in a direction favorable for substrate binding. One possibility for why no enhanced luciferase performance was observed could be that when the SC-LumiLuc and SC-LumiScarlet proteins were bound to the ST-E2, the luciferase protein conformation was slightly altered. In addition to the substrate binding site, other residues on the LumiLuc such as residue G4 at the N-terminus and H164 at the C-terminus of LumiLuc were shown to play a role in the enhanced light output

of LumiLuc-8pyDTZ [12]. Since the N-terminus of LumiLuc is fused to SpyCatcher and the C-terminus of LumiLuc is also oriented near the N-terminus, the presence of the SpyCatcher could affect the intermolecular binding interactions of the luciferase when conjugated to ST-E2.

The immobilization of LumiScarlet onto E2 resulted in red-shifted bioluminescent nanoparticles that can be used for bioimaging to better visualize nanoparticle pharmacokinetics and biodistribution *in vivo.* Conventional bioimaging techniques to assay pharmacological behavior of nanoparticles for drug delivery and therapeutics utilize fluorescent particles and fluorescent imaging [52,53,54]. Yet, the tendency of fluorophores to undergo photobleaching and for tissues to produce autofluorescence limits the sensitivity of fluorescence imaging and can affect the interpretation of results, even when using red-shifted fluorophores [52]. In a study that assessed the *in vivo* bioimaging performance of fluorescent E2 particles loaded with conventional red fluorescent molecules compared to bioluminescent Nluc-E2 particles, the fluorescent E2 particles produced high background and much lower signal-to-noise ratios compared to Nluc-E2 [28]. In contrast to the red fluorescent E2, LumiScarlet-E2 could serve as a more sensitive red-shifted nanoparticle for bioimaging, as bioluminescence-based emission produces low background with high signal-to-noise ratios [4].

3.6. LumiScarlet-E2 exhibited the most red-shifted emission compared to CeNLuc-E2, LumiLuc-E2, and Nluc-E2

Next, we compared the luminescent properties of CeNLuc-E2, Nluc-E2, LumiScarlet-E2, and LumiLuc-E2. In addition to measuring the total luminescence of all the particles (Figure 12a), we concurrently measured their red-shifted luminescence (Figure 12b). The DsRed filter, which measures red-shifted emission from 575-650 nm, was used with IVIS to assess the particles' deep tissue penetration capacity as more red-shifted wavelengths exhibit improved

tissue penetration [16]. First, comparing the total luminescence of CeNLuc-E2, Nluc-E2, LumiScarlet-E2, and LumiLuc-E2 particles, both the LumiScarlet-E2 and LumiLuc-E2 particles exhibited a significantly lower flux than both CeNLuc-E2 and Nluc-E2 (Figure 12a). This was in contrast to the soluble LumiScarlet and LumiLuc proteins, which both displayed a total luminescence that was comparable to Nluc (Figure S8). LumiScarlet also exhibited a significantly greater total luminescence than CeNLuc (Figure S8). Comparing the BRET-based nanoparticles, CeNLuc-E2 was 3.5-fold brighter than LumiScarlet-E2 and comparing the luciferase-only nanoparticles, Nluc-E2 was 4.6-fold brighter than LumiLuc-E2 (Figure 12a).

In contrast, when analyzing the red-shifted emissions of all the particles using the DsRed filter, LumiScarlet-E2 exhibited significantly greater emission than CeNLuc-E2, Nluc-E2, and LumiLuc-E2 (Figure 12b). Similarly, unconjugated LumiScarlet and SC-LumiScarlet displayed the greatest red-shifted emission out of all the luminescent proteins (Figure S9). LumiScarlet-E2 exhibited the most red-shifted spectral profile of all the particles, peaking at 595 nm (Figure 7b). As a result, a significantly greater proportion of the LumiScarlet-E2 emission consisted of emission in the red-shifted range compared to the rest of the luminescent particles (Figure 12c).

Comparing the BRET-based nanoparticles, LumiScarlet-E2 produced a 4-fold greater flux than CeNLuc-E2 using the DsRed filter (Figure 12b). Although the total luminescence of LumiScarlet-E2 is still lower than CeNLuc-E2 (Figure 12a), the luminescence output between the two could vary *in vivo* because red wavelength light penetrates more readily through tissues than blue light [16,55]. In studies assessing the effect of tissue absorption on the emission of luciferases expressed in cells and expressed *in vivo* at different tissue depths, luciferases with red-shifted emissions displayed bioluminescent signals that were less absorbed by mammalian tissue than luciferases with blue-shifted emissions [16,56]. Therefore, LumiScarlet-E2 could

exhibit increased tissue penetration than CeNLuc-E2.
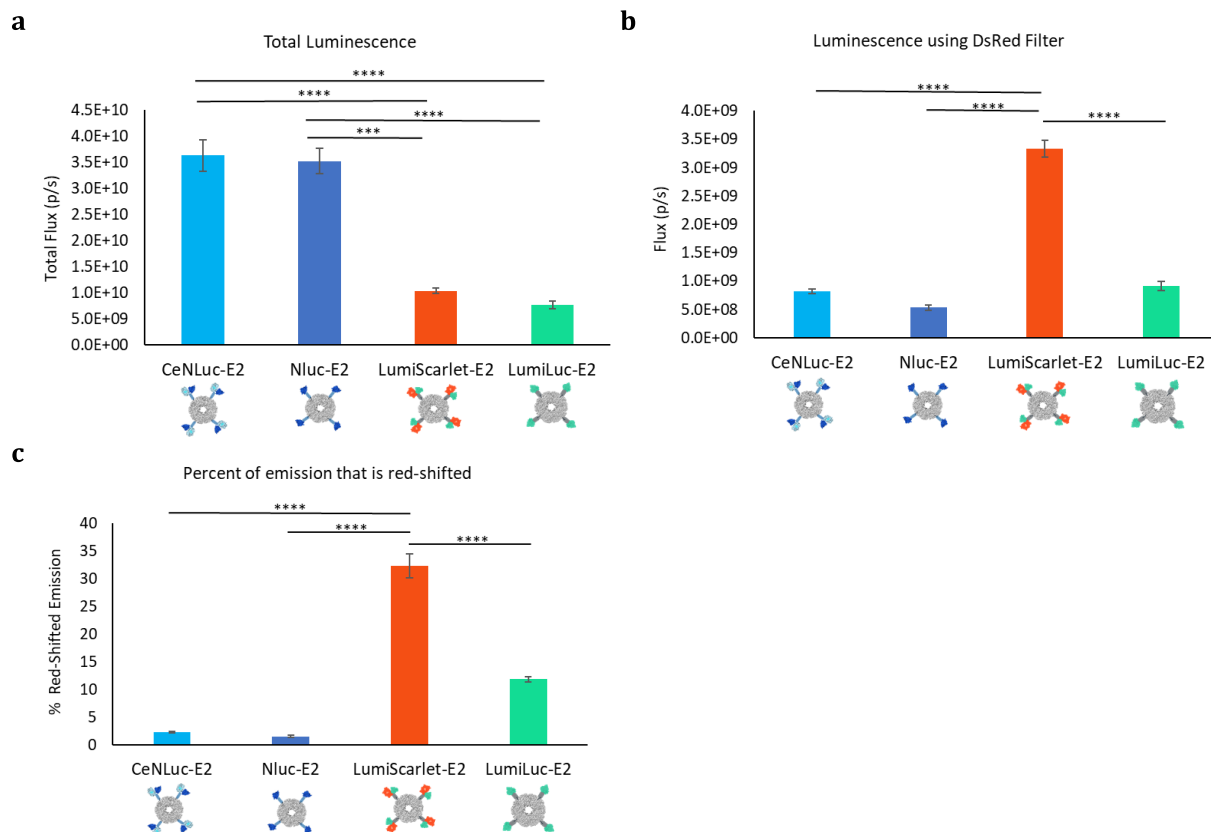
Figure 12. Comparison of BRET-fusion reporter conjugated particles and luciferase conjugated particles. a) Total luminescence of CeNLuc-E2, Nluc-E2, LumiScarlet-E2, and LumiLuc-E2. CeNLuc-E2 and Nluc-E2 received FRZ substrate and LumiScarlet-E2 and LumiLuc-E2 received 8pyDTZ b) Red-shifted luminescence of particles using the DsRed filter (Em 575- 650 nm). c) Quantification of the proportion of total emission that is red-shifted. All data is represented as mean ± SEM of n=3 independent experiments, with background subtracted. One-way ANOVA with Tukey's multiple comparison test were performed (***$p < .001$,****$p < 0.0001$).

Similarly, although LumiLuc-E2 was less bright than Nluc-E2, it consisted of a greater proportion of red-shifted emission and could exhibit improved tissue penetration than Nluc-E2 (Figure 12c). Furthermore, LumiLuc-E2 and LumiScarlet-E2 utilize 8pyDTZ substrate which has enhanced water solubility compared to conventional substrates and can be administered at high doses *in vivo,* which make them more advantageous for *in vivo* use [12]. Collectively, these

factors suggest that LumiScarlet-E2 and LumiLuc-E2 can still serve as effective bioimaging reporters for *in vivo* applications. However, the *in vivo* luminescence of the luminescent particles remains to be assayed to more accurately determine the deep tissue penetration capacity of the particles.

4. CONCLUSIONS

The aim of this study was to develop brighter and more red-shifted bioluminescent reporters to address the challenges of reduced signal intensity and sensitivity in *in vivo* BLI. We conjugated BRET-based fusion reporters, namely CeNLuc and LumiScarlet, directly to the surface of E2 nanoparticles to produce an effective imaging platform that luminesced as a result of efficient bioluminescence resonance energy transfer between the donor and acceptor molecules of the fusion reporters. We demonstrated that CeNLuc and LumiScarlet could be successfully immobilized onto the E2 nanoparticle surface using the SpyCatcher-SpyTag conjugation method. Moreover, we could control the ratio of luminescent proteins conjugated to a nanoparticle.

Our luminescence assays revealed that CeNLuc-E2 produced an enhanced luminescence output compared to unconjugated CeNLuc proteins, suggesting that immobilizing CeNLuc onto E2 improved luminescence, resulting in a brighter reporter. We also designed bioluminescent E2 nanoparticles that produced a red-shifted emission through BRET to address the need for reporters that can enable more sensitive deep tissue imaging. LumiScarlet-E2 exhibited substantially better luminescent properties in the red-shifted spectrum than CeNLuc-E2, demonstrating LumiScarlet-E2's potential for improved deep tissue penetration.

Since this study only assessed the *in vitro* luminescence performance of CeNLuc-E2 and LumiScarlet-E2, the *in vivo* performance of the BRET-based particles remains to be elucidated to more accurately assess the particles' deep tissue imaging capacity. Nonetheless, the optimal imaging properties displayed by CeNLuc-E2 and LumiScarlet-E2 demonstrate their potential as sensitive imaging reporters that can be utilized for broad *in vivo* applications such as biodistribution or tracking studies.

5. FUTURE WORK

In this thesis work, the luminescence of CeNLuc-E2 and LumiScarlet-E2 was assessed through *in vitro* protein-based assays. However, to evaluate the imaging properties of the particles for *in vivo* BLI with more accuracy, it would be advantageous to observe luminescence of the particles in an *in vivo* model. We can better visualize whether the red-shifted LumiScarlet-E2 exhibits improved emission compared to the blue-shifted CeNLuc-E2 *in vivo*. Although the *in vitro* luminescence of LumiScarlet-E2 was lower than CeNLuc-E2, the *in vivo* luminescence could yield different results as red-shifted light is less attenuated by tissue and has shown improved *in vivo* bioimaging [16]. For instance, in a study comparing the luminescence of LumiLuc to LumiScarlet, no significant difference was observed *in vitro*, however *in vivo*, the signal of LumiScarlet was significantly greater than LumiLuc due to its more red-shifted emission [12]. Furthermore, Nluc-E2 has already shown efficient imaging properties *in vivo*, producing sensitive signals with high signal-to-noise ratios. LumiScarlet-E2 could potentially enhance the signal sensitivity, as its more red-shifted emission would be less absorbed and scattered by tissue. Therefore, assaying the *in vivo* performance would help better determine the capability of CeNLuc-E2 and LumiScarlet-E2 as improved bioimaging reporters.

REFERENCES

1. Zambito, G., Chawda, C., & Mezzanotte, L. Emerging tools for bioluminescence imaging. *Current Opinion in Chemical Biology* **63**, 86-94, doi:10.1016/j.cbpa.2021.02.005 (2021).

2. England, C. G., Ehlerding, E. B., & Cai, W. NanoLuc: A small luciferase is brightening up the field of bioluminescence. *Bioconjugate Chemistry* **27**, 1175-1187, doi:10.1021/acs.bioconjchem.6b00112 (2016).

3. Love, A. C., & Prescher, J. A. Seeing (and Using) the Light: Recent developments in Bioluminescence Technology. *Cell Chemical Biology* **27**, 904-920, doi:10.1016/j.chembiol.2020.07.022 (2020).

4. Ozawa, T., Yoshimura, H., & Kim, S. B. Advances in fluorescence and bioluminescence imaging. *Analytical Chemistry* **85**, 590-609, doi:10.1021/ac3031724 (2012).

5. Suzuki, K., Kimura, T., Shinoda, H., Bai, G., Daniels, M. J., Arai, Y., et al. Five colour variants of bright luminescent protein for real-time multicolour bioimaging. *Nature Communications* **7**, doi:10.1038/ncomms13718 (2016).

6. Weissleder, R., & Ntziachristos, V. Shedding light onto live molecular targets. *Nature Medicine* **9**, 123–128, doi:10.1038/nm0103-123 (2003).

7. Mezzanotte, L., Van 't Root, M., Karatas, H., Goun, E. A., & Löwik, C. W. In vivo molecular bioluminescence imaging: New Tools and Applications. *Trends in Biotechnology* **35**, 640-652, doi:10.1016/j.tibtech.2017.03.012 (2017).

8. Shah, K., & Weissleder, R. Molecular optical imaging: Applications leading to the development of present day therapeutics. *NeuroRX* **2**, 215-225, doi:10.1602/neurorx.2.2.215 (2005).

9. Yeh, H., Karmach, O., Ji, A., Carter, D., Martins-Green, M. M., & Ai, H. Red-shifted luciferase–luciferin pairs for enhanced bioluminescence imaging. *Nature Methods* **14**, 971-974, doi:10.1038/nmeth.4400 (2017).

10. Bhaumik, S., & Gambhir, S. S. Optical imaging of *Renilla* luciferase reporter gene expression in living mice. *Proceedings of the National Academy of Sciences* **99**, 377-382, doi:10.1073/pnas.012611099 (2001).

11. Tisi, L. C., White, P. J., Squirrell, D. J., Murphy, M. J., Lowe, C. R., & Murray, J. A. H. Development of a thermostable firefly luciferase. *Analytica Chimica Acta* **457**, 115–123, doi:10.1016/s0003-2670(01)01496-9 (2002).

12. Yeh, H., Xiong, Y., Wu, T., Chen, M., Ji, A., Li, X., & Ai, H. ATP-independent bioluminescent reporter variants to improve *in vivo* imaging. *ACS Chemical Biology* **14**, 959-965, doi:10.1021/acschembio.9b00150 (2019).

13. Hall, M. P., Unch, J., Binkowski, B. F., Valley, M. P., Butler, B. L., Wood, M. G., et al. Engineered luciferase reporter from a deep sea shrimp utilizing a novel imidazopyrazinone substrate. *ACS Chemical Biology* **7**, 1848–1857, doi:10.1021/cb3002478 (2012).

14. Dale, N. C., Johnstone, E. K., White, C. W., & Pfleger, K. D. NanoBRET: The bright future of proximity-based assays. *Frontiers in Bioengineering and Biotechnology* **7**, doi:10.3389/fbioe.2019.00056 (2019).

15. Xiong, Y., Zhang, Y., Li, Z., Reza, M. S., Li, X., Tian, X., & Ai, H. Engineered amber-emitting nano luciferase and its use for immunobioluminescence imaging *in vivo*. *Journal of the American Chemical Society* **144**, 14101–14111, doi:10.1021/jacs.2c02320 (2022).

16. Zhao, H., Doyle, T. C., Coquoz, O., Kalish, F., Rice, B. W., & Contag, C. H. Emission spectra of bioluminescent reporters and interaction with mammalian tissue determine the sensitivity of detection in vivo. *Journal of Biomedical Optics* **10**, 041210. doi:10.1117/1.2032388 (2005).

17. Liu, S., Su, Y., Lin, M. Z., & Ronald, J. A. Brightening up biology: Advances in luciferase systems for *in vivo* imaging. *ACS Chemical Biology* **16**(12), 2707–2718, doi:10.1021/acschembio.1c00549 (2021).

18. Yeh, H., & Ai, H. Development and applications of bioluminescent and chemiluminescent reporters and biosensors. *Annual Review of Analytical Chemistry* **12**, 129-150, doi:10.1146/annurev-anchem-061318-115027 (2019).

19. Kobayashi, H., Picard, L., Schönegge, A., & Bouvier, M. Bioluminescence resonance energy transfer–based imaging of protein–protein interactions in living cells. *Nature Protocols* **14**, 1084-1107. doi:10.1038/s41596-019-0129-7 (2019).

20. Xie, Q., Soutto, M., Xu, X., Zhang, Y., & Johnson, C. H. Bioluminescence Resonance Energy Transfer (BRET) imaging in plant seedlings and mammalian cells. *Methods in Molecular Biology*, 3–28, doi:10.1007/978-1-60761-901-7_1 (2010).

21. Weihs, F., Wang, J., Pfleger, K. D., & Dacres, H. Experimental determination of the Bioluminescence Resonance Energy Transfer (BRET) förster distances of nanobret and red-shifted Bret Pairs. *Analytica Chimica Acta: X* **6**, 100059. doi:10.1016/j.acax.2020.100059 (2020).

22. Borroto-Escuela, D. O., Flajolet, M., Agnati, L. F., Greengard, P., & Fuxe, K. Bioluminescence resonance energy transfer methods to study G protein-coupled

receptor–receptor tyrosine kinase heteroreceptor complexes. *Methods in Cell Biology*, 141–164, doi:10.1016/b978-0-12-408143-7.00008-6 (2013).

23. Takai, A., Nakano, M., Saito, K., Haruno, R., Watanabe, T. M., Ohyanagi, T., et al. Expanded palette of nano-lanterns for real-time multicolor Luminescence Imaging. *Proceedings of the National Academy of Sciences* **112**, 4352–4356, doi:10.1073/pnas.1418468112 (2015).

24. Chu, J., Oh, Y., Sens, A., Ataie, N., Dana, H., Macklin, J. J., et al. A bright cyan-excitable orange fluorescent protein facilitates dual-emission microscopy and enhances bioluminescence imaging in vivo. *Nature Biotechnology* **34**, 760–767, doi:10.1038/nbt.3550 (2016).

25. Schaub, F. X., Reza, M. S., Flaveny, C. A., Li, W., Musicant, A. M., et al. Fluorophore-NanoLuc Bret reporters enable sensitive *in vivo* optical imaging and flow cytometry for monitoring tumorigenesis. *Cancer Research* **75**, 5023-5033, doi:10.1158/0008-5472.can-14-3538 (2015).

26. Parag-Sharma, K., O'Banion, C. P., Henry, E. C., Musicant, A. M., Cleveland, J. L., Lawrence, D. S., & Amelio, A. L. Engineered Bret-based biologic light sources enable spatiotemporal control over diverse optogenetic systems. *ACS Synthetic Biology* **9**, 1-9 doi:10.1021/acssynbio.9b00277 (2019).

27. Wang, F., Yang, K., Wang, Z., Ma, Y., Gutkind, J. S., Hida, N., et al. Combined image guided monitoring the pharmacokinetics of rapamycin loaded human serum albumin nanoparticles with a split luciferase reporter. *Nanoscale* **8**, 3991-4000, doi:10.1039/c5nr07308a (2016).

28. Li, E., Brennan, C. K., Ramirez, A., Tucker, J. A., Butkovich, N., Meli, V. S., et al. Macromolecular Assembly of bioluminescent protein nanoparticles for enhanced imaging. *Materials Today Bio* **17**, doi:10.1016/j.mtbio.2022.100455 (2022).

29. Jia, L., Minamihata, K., Ichinose, H., Tsumoto, K., & Kamiya, N. Polymeric Spycatcher scaffold enables bioconjugation in a ratio-controllable manner. *Biotechnology Journal* **12**, doi:10.1002/biot.201700195 (2017).

30. Ding, S., Cargill, A. A., Medintz, I. L., & Claussen, J. C. Increasing the activity of immobilized enzymes with nanoparticle conjugation. *Current Opinion in Biotechnology* **34**, 242-250, doi:10.1016/j.copbio.2015.04.005 (2015).

31. Kamkaew, A., Sun, H., England, C. G., Cheng, L., Liu, Z., & Cai, W. Quantum Dot–NanoLuc bioluminescence resonance energy transfer enables tumor imaging and lymph node mapping in vivo. *Chemical Communications* **52**, 6997-7000, doi:10.1039/c6cc02764d (2016).

32. Alam, R., Karam, L. M., Doane, T. L., Coopersmith, K., Fontaine, D. M., Branchini, B. R., & Maye, M. M. Probing bioluminescence resonance energy transfer in quantum rod–luciferase nanoconjugates. *ACS Nano* **10**, 1969–1977, doi:10.1021/acsnano.5b05966 (2016).

33. Fan, Q., Dehankar, A., Porter, T. K., & Winter, J. O. Effect of micelle encapsulation on toxicity of CdSe/Zns and Mn-doped ZnSe Quantum Dots. *Coatings* **11**, 895, doi:10.3390/coatings11080895 (2021).

34. Tang, Y., Han, S., Liu, H., Chen, X., Huang, L., Li, X., & Zhang, J. The role of surface chemistry in determining in vivo biodistribution and toxicity of CdSe/ZnS core–shell

quantum dots. *Biomaterials* **34**, 8741-8755,doi:10.1016/j.biomaterials.2013.07.087 (2013).

35. Lu, L., Li, B., Ding, S., Fan, Y., Wang, S., Sun, C., et al. Nir-II bioluminescence for in vivo high contrast imaging and in situ ATP-mediated metastases tracing. *Nature Communications* **11**, doi:10.1038/s41467-020-18051-1 (2020).

36. Yang, Y., Hou, W., Liu, S., Sun, K., Li, M., & Wu, C. Biodegradable polymer nanoparticles for photodynamic therapy by Bioluminescence Resonance Energy Transfer. *Biomacromolecules* **19**, 201-208, doi:10.1021/acs.biomac.7b01469 (2017).

37. Yan, H., Forward, S., Kim, K., Wu, Y., Hui, J., Kashiparekh, A., & Yun, S. All-natural-molecule, bioluminescent photodynamic therapy results in complete tumor regression and prevents metastasis. *Biomaterials* **296**, 122079. doi:10.1016/j.biomaterials.2023.122079 (2023).

38. Dalmau, M., Lim, S., Chen, H. C., Ruiz, C., & Wang, S. Thermostability and molecular encapsulation within an engineered caged protein scaffold. *Biotechnology and Bioengineering* **101**, 654-664, doi:10.1002/bit.21988 (2008).

39. Butkovich, N., Li, E., Ramirez, A., Burkhardt, A. M., & Wang, S. Advancements in protein nanoparticle vaccine platforms to combat infectious disease. *WIREs Nanomedicine and Nanobiotechnology* **13**, doi:10.1002/wnan.1681 (2020).

40. Markwardt, M. L., Kremers, G.-J., Kraft, C. A., Ray, K., Cranfill, P. J., Wilson, K. A., et al. An improved cerulean fluorescent protein with enhanced brightness and reduced reversible photoswitching. *PLoS ONE* **6**, doi:10.1371/journal.pone.0017896 (2011).

41. Bindels, D. S., Haarbosch, L., van Weeren, L., Postma, M., Wiese, K. E., Mastop, M., et al. mScarlet: A bright monomeric red fluorescent protein for cellular imaging. *Nature Methods* **14**, 53–56, doi:10.1038/nmeth.4074 (2016).

42. Lorenz, T. C. Polymerase chain reaction: Basic protocol plus troubleshooting and optimization strategies. *Journal of Visualized Experiments*, doi:10.3791/3998 (2012).

43. Zakeri, B., Fierer, J. O., Celik, E., Chittock, E. C., Schwarz-Linek, U., Moy, V. T., & Howarth, M. Peptide tag forming a rapid covalent bond to a protein, through engineering a bacterial adhesin. *Proceedings of the National Academy of Sciences* **109**, doi:10.1073/pnas.1115485109 (2012).

44. Thrane, S., Janitzek, C. M., Matondo, S., Resende, M., Gustavsson, T., de Jongh, W. A., et al. Bacterial superglue enables easy development of efficient virus-like particle based vaccines. *Journal of Nanobiotechnology* **14**, doi:10.1186/s12951-016-0181-1 (2016).

45. Xu, Y., Piston, D. W., & Johnson, C. H. A Bioluminescence Resonance Energy Transfer (BRET) system: Application to interacting circadian clock proteins. *Proceedings of the National Academy of Sciences* **96**, 151–156, doi:10.1073/pnas.96.1.151 (1999).

46. Izard, T., Ævarsson, A., Allen, M. D., Westphal, A. H., Perham, R. N., de Kok, A., & Hol, W. G. Principles of quasi-equivalence and Euclidean geometry govern the assembly of cubic and dodecahedral cores of pyruvate dehydrogenase complexes. *Proceedings of the National Academy of Sciences* **96**, 1240–1245, doi:10.1073/pnas.96.4.1240 (1999).

47. Day, R. N., & Davidson, M. W. Fluorescent proteins for FRET microscopy: Monitoring protein interactions in living cells. *BioEssays* **34**(5), 341–350, doi:10.1002/bies.201100098 (2012).

48. Stryer, L. Fluorescence energy transfer as a spectroscopic ruler. *Annual Review of Biochemistry* **47**(1), 819–846, doi:10.1146/annurev.bi.47.070178.004131 (1978).

49. Yang, F., Moss, L. G., & Phillips, G. N. The molecular structure of green fluorescent protein. *Nature Biotechnology* **14**, 1246–1251, doi:10.1038/nbt1096-1246 (1996).

50. Li, F., Yu, J., Zhang, Z., Cui, Z., Wang, D., Wei, H., & Zhang, X. Buffer enhanced bioluminescence resonance energy transfer sensor based on GAUSSIA luciferase for in vitro detection of protease. *Analytica Chimica Acta* **724**, 104-110, doi:10.1016/j.aca.2012.02.047 (2012).

51. Ugarova, N. N. Interaction of firefly luciferase with substrates and their analogs: A study using fluorescence spectroscopy methods. *Photochemical & Photobiological Sciences* **7**, 218–227, doi:10.1039/b712895a (2008).

52. Arms, L., Smith, D. W., Flynn, J., Palmer, W., Martin, A., Woldu, A., & Hua, S. Advantages and limitations of current techniques for analyzing the biodistribution of nanoparticles. *Frontiers in Pharmacology* **9**, doi:10.3389/fphar.2018.00802 (2018).

53. Pratiwi, F. W., Kuo, C. W., Chen, B.-C., & Chen, P. Recent advances in the use of fluorescent nanoparticles for bioimaging. *Nanomedicine* **14**, 1759–1769,doi:10.2217/nnm-2019-0105 (2019).

54. Priem, B., Tian, C., Tang, J., Zhao, Y., & Mulder, W. J. Fluorescent nanoparticles for the accurate detection of drug delivery. *Expert Opinion on Drug Delivery* **12**, 1881–1894, doi:10.1517/17425247.2015.1074567 (2015).

55. Rice, B. W., Cable, M. D., & Nelson, M. B. In vivo imaging of light-emitting probes. *Journal of Biomedical Optics* **6**, 432, doi:10.1117/1.1413210 (2001).

56. Liang, Y., Bulte, J. W., & Walczak, P. Comparison of red-shifted firefly luciferase ppy RE9 and conventional LUC2 as bioluminescence imaging reporter genes for in vivo imaging of stem cells. *Journal of Biomedical Optics* **17**(1), doi:10.1117/1.jbo.17.1.016004 (2012).

APPENDICES

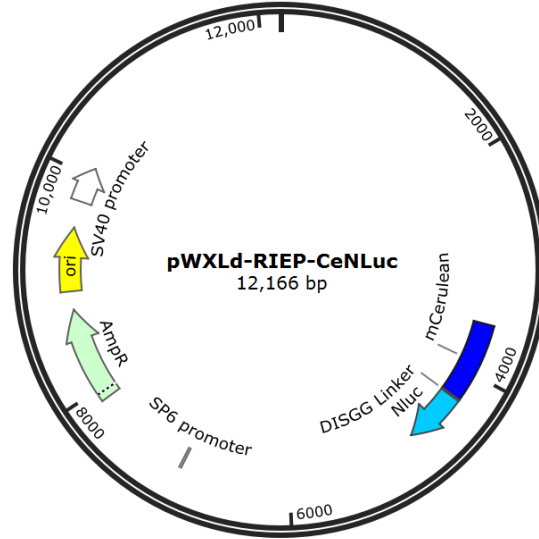**Appendix A. Plasmid maps of original CeNLuc and LumiScarlet plasmids**

Figure A1. Original plasmid containing CeNLuc gene (Addgene plasmid #135934).
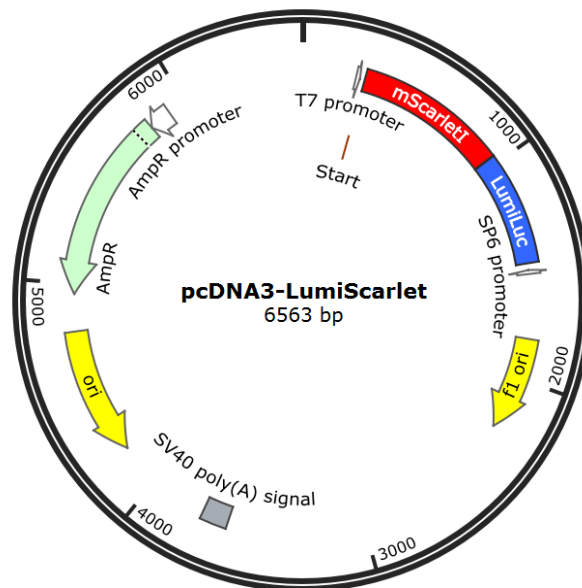

Figure A2. Original plasmid containing LumiScarlet gene (Addgene plasmid #126623).

Appendix B. Oligonucleotides used in this study

Primer Name	Oligonucleotide Sequence (5' to 3')
NheI-spacer-mScarletI F	GCTAGCGGT TCA GGA ACA GCA GGT GGT GGG TCA GGT TCC GTG AGC AAG GGC GAG GCA
BamHI-stop-mScarletI R	GGATCCTTA TCC GGT GGA GTG GCG G
NheI-spacer-LumiLuc F	GCTAGC GGT TCA GGA ACA GCA GGT GGT GGG TCA GGT TCC ACT CTC GGG GAT TTT GTT GGG G
BamHI-stop-LumiLuc R	GGATCCTTA CGC CAG AAT GCG TTC ATG CAG
NheI-start-6x His Tag- mScarletI F	GCTAGC ATG CAT CAT CAC CAT CAC CAC GTG AGC AAG GGC GAG GCA
NheI-start- 6x His Tag- LumiLuc F	GCTAGC ATG CAT CAT CAC CAT CAC CAC ACT CTC GGG GAT TTT GTT GGG G
NheI-spacer- mCerulean3 F	GCTAGC GGT TCA GGA ACA GCA GGT GGT GGG TCA GGT TCC GTG AGC AAG GGC GAG GAG C
BamHI-stop-mCerulean3 R	GGATCC TTA CTT GTA CAG CTC GTC CAT GCC G
BamHI-stop-Nluc R	GGATCC TTA CGC CAG AAT GCG TTC GCA CAG
NheI-6x His Tag- mCerulean3 F	GGATCC TTA CTT GTA CAG CTC GTC CAT GCC G

Appendix C. Plasmid maps of cloned CeNLuc and LumiScarlet constructs
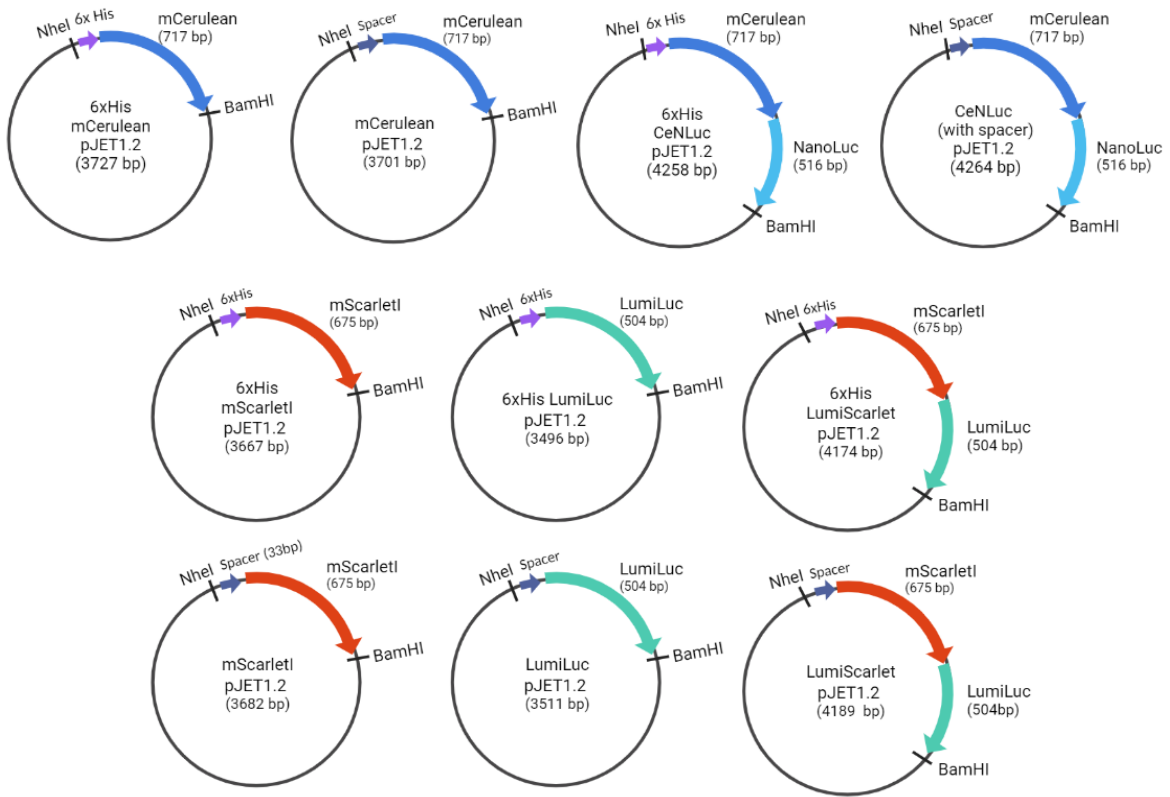
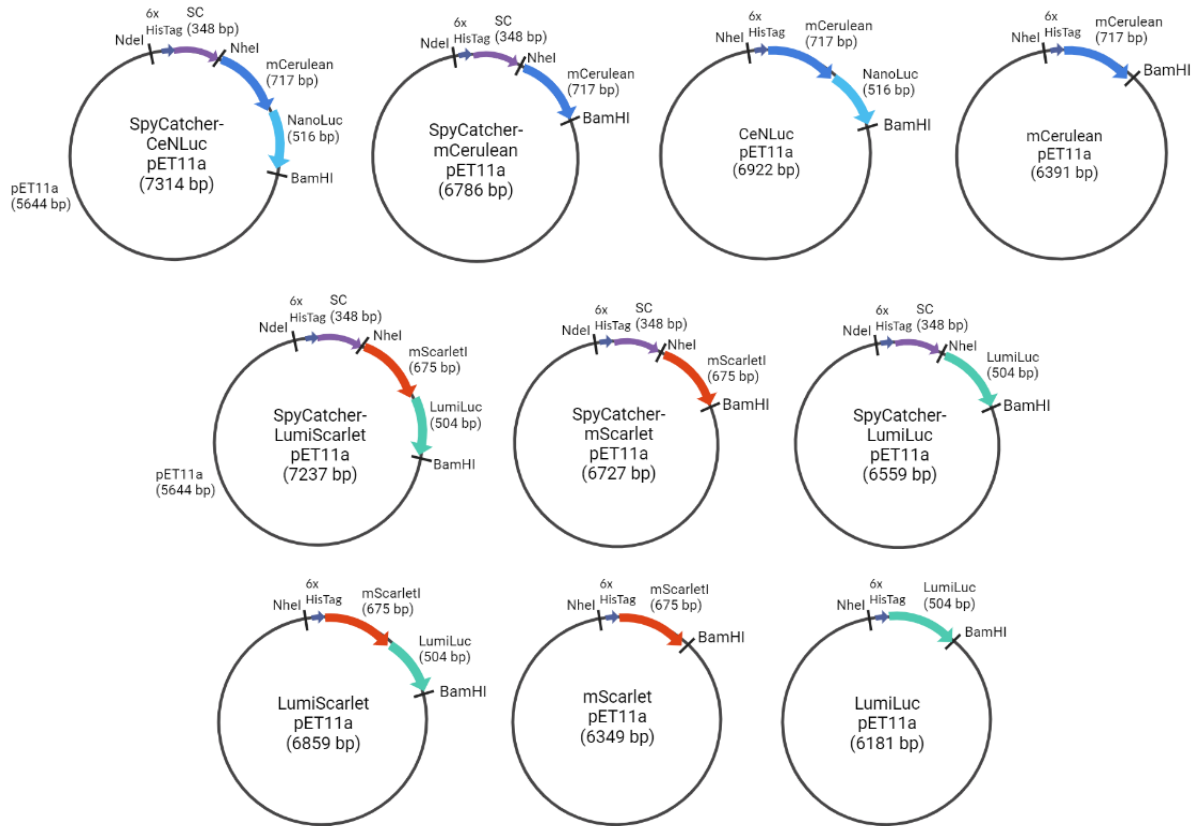

Figure C1. Plasmid maps of constructs in pJET1.2 vector.

Figure C2. Constructs in pET11-SpyCatcher or pET11a vector.

Appendix D. DNA sequences of cloned constructs

Construct	Sequence (5' to 3')
6x HisTag-CeNLuc	CATCATCACCATCACCACGTGAGCAAGGGCGAGGAGCTGTTCACCGGGGTGGT GCCCATCCTGGTCGAGCTGGACGGCGACGTAAACGGCCACAAGTTCAGCGTGT CCGGCGAGGGCGAGGGCGATGCCACCTACGGCAAGCTGACCCTGAAGTTCATC TGCACCACCGGCAAGCTGCCCGTGCCCTGGCCCACCCTCGTGACCACCCTGAG CTGGGGCGTGCAGTGCTTCGCCCGCTACCCCGACCACATGAAGCAGCACGACT TCTTCAAGTCCGCCATGCCCGAAGGCTACGTCCAGGAGCGCACCATCTTCTTCA AGGACGACGGCAACTACAAGACCCGCGCCGAGGTGAAGTTCGAGGGCGACAC CCTGGTGAACCGCATCGAGCTGAAGGGCATCGACTTCAAGGAGGACGGCAAC ATCCTGGGGCACAAGCTGGAGTACAACGCCATCCACGGCAACGTCTATATCACC GCCGACAAGCAGAAGAACGGCATCAAGGCCAACTTCGGCCTCAACTGCAACAT CGAGGACGGCAGCGTGCAGCTCGCCGACCACTACCAGCAGAACACCCCCATCG GCGACGGCCCCGTGCTGCTGCCCGACAACCACTACCTGAGCACCCAGTCCAAG CTGAGCAAAGACCCCAACGAGAAGCGCGATCACATGGTCCTGCTGGAGTTCGT GACCGCCGCCGGGATCACTCTCGGCATGGACGAGCTGTACAAGGATATCTCCGG AGGTATGGTCTTCACACTCGAAGATTTCGTTGGGGACTGGCGACAGACAGCCG GCTACAACCTGGACCAAGTCCTTGAACAGGGAGGTGTGTCCAGTTTGTTTCAG AATCTCGGGGTGTCCGTAACTCCGATCCAAAGGATTGTCCTGAGCGGTGAAAAT GGGCTGAAGATCGACATCCATGTCATCATCCCGTATGAAGGTCTGAGCGGCGAC CAAATGGGCCAGATCGAAAAAATTTTTAAGGTGGTGTACCCTGTGGATGATCAT CACTTTAAGGTGATCCTGCACTATGGCACACTGGTAATCGACGGGGTTACGCCG AACATGATCGACTATTTCGGACGGCCGTATGAAGGCATCGCCGTGTTCGACGGC AAAAAGATCACTGTAACAGGGACCCTGTGGAACGGCAACAAAATTATCGACGA GCGCCTGATCAACCCCGACGGCTCCCTGCTGTTCCGAGTAACCATCAACGGAG TGACCGGCTGGCGGCTGTGCGAACGCATTCTGGCGTAA
Spacer-CeNLuc	GGTTCAGGAACAGCAGGTGGTGGGTCAGGTTCCGTGAGCAAGGGCGAGGAGC TGTTCACCGGGGTGGTGCCCATCCTGGTCGAGCTGGACGGCGACGTAAACGGC CACAAGTTCAGCGTGTCCGGCGAGGGCGAGGGCGATGCCACCTACGGCAAGCT GACCCTGAAGTTCATCTGCACCACCGGCAAGCTGCCCGTGCCCTGGCCCACCC TCGTGACCACCCTGAGCTGGGGCGTGCAGTGCTTCGCCCGCTACCCCGACCAC ATGAAGCAGCACGACTTCTTCAAGTCCGCCATGCCCGAAGGCTACGTCCAGGA GCGCACCATCTTCTTCAAGGACGACGGCAACTACAAGACCCGCGCCGAGGTGA AGTTCGAGGGCGACACCCTGGTGAACCGCATCGAGCTGAAGGGCATCGACTTC AAGGAGGACGGCAACATCCTGGGGCACAAGCTGGAGTACAACGCCATCCACG GCAACGTCTATATCACCGCCGACAAGCAGAAGAACGGCATCAAGGCCAACTTC GGCCTCAACTGCAACATCGAGGACGGCAGCGTGCAGCTCGCCGACCACTACCA GCAGAACACCCCCATCGGCGACGGCCCCGTGCTGCTGCCCGACAACCACTACC TGAGCACCCAGTCCAAGCTGAGCAAAGACCCCAACGAGAAGCGCGATCACAT GGTCCTGCTGGAGTTCGTGACCGCCGCCGGGATCACTCTCGGCATGGACGAGC TGTACAAGGATATCTCCGGAGGTATGGTCTTCACACTCGAAGATTTCGTTGGGG ACTGGCGACAGACAGCCGGCTACAACCTGGACCAAGTCCTTGAACAGGGAGG TGTGTCCAGTTTGTTTCAGAATCTCGGGGTGTCCGTAACTCCGATCCAAAGGAT TGTCCTGAGCGGTGAAAATGGGCTGAAGATCGACATCCATGTCATCATCCCGTA TGAAGGTCTGAGCGGCGACCAAATGGGCCAGATCGAAAAAATTTTTAAGGTGG TGTACCCTGTGGATGATCATCACTTTAAGGTGATCCTGCACTATGGCACACTGGT AATCGACGGGGTTACGCCGAACATGATCGACTATTTCGGACGGCCGTATGAAGG CATCGCCGTGTTCGACGGCAAAAAGATCACTGTAACAGGGACCCTGTGGAACG GCAACAAAATTATCGACGAGCGCCTGATCAACCCCGACGGCTCCCTGCTGTTCC GAGTAACCATCAACGGAGTGACCGGCTGGCGGCTGTGCGAACGCATTCTGGCG TAA

6x HisTag- mCerulean3	CATCATCACCATCACCACGTGAGCAAGGGCGAGGAGCTGTTCACCGGGGGTGGT GCCCATCCTGGTCGAGCTGGACGGCGACGTAAACGGCCACAAGTTCAGCGTGT CCGGCGAGGGCGAGGGCGATGCCACCTACGGCAAGCTGACCCTGAAGTTCATC TGCACCACCGGCAAGCTGCCCGTGCCCTGGCCCACCCTCGTGACCACCCTGAG CTGGGGCGTGCAGTGCTTCGCCCGCTACCCCGACCACATGAAGCAGCACGACT TCTTCAAGTCCGCCATGCCCGAAGGCTACGTCCAGGAGCGCACCATCTTCTTCA AGGACGACGGCAACTACAAGACCCGCGCCGAGGTGAAGTTCGAGGGCGACAC CCTGGTGAACCGCATCGAGCTGAAGGGCATCGACTTCAAGGAGGACGGCAAC ATCCTGGGGCACAAGCTGGAGTACAACGCCATCCACGGCAACGTCTATATCACC GCCGACAAGCAGAAGAACGGCATCAAGGCCAACTTCGGCCTCAACTGCAACAT CGAGGACGGCAGCGTGCAGCTCGCCGACCACTACCAGCAGAACACCCCCATCG GCGACGGCCCCGTGCTGCTGCCCGACAACCACTACCTGAGCACCCAGTCCAAG CTGAGCAAAGACCCCAACGAGAAGCGCGATCACATGGTCCTGCTGGAGTTCGT GACCGCCGCCGGGATCACTCTCGGCATGGACGAGCTGTACAAG
Spacer- mCerulean3	GGTTCAGGAACAGCAGGTGGTGGGTCAGGTTCCGTGAGCAAGGGCGAGGAGC TGTTCACCGGGGGTGGTGCCCATCCTGGTCGAGCTGGACGGCGACGTAAACGGC CACAAGTTCAGCGTGTCCGGCGAGGGCGAGGGCGATGCCACCTACGGCAAGCT GACCCTGAAGTTCATCTGCACCACCGGCAAGCTGCCCGTGCCCTGGCCCACCC TCGTGACCACCCTGAGCTGGGGCGTGCAGTGCTTCGCCCGCTACCCCGACCAC ATGAAGCAGCACGACTTCTTCAAGTCCGCCATGCCCGAAGGCTACGTCCAGGA GCGCACCATCTTCTTCAAGGACGACGGCAACTACAAGACCCGCGCCGAGGTGA AGTTCGAGGGCGACACCCTGGTGAACCGCATCGAGCTGAAGGGCATCGACTTC AAGGAGGACGGCAACATCCTGGGGCACAAGCTGGAGTACAACGCCATCCACG GCAACGTCTATATCACCGCCGACAAGCAGAAGAACGGCATCAAGGCCAACTTC GGCCTCAACTGCAACATCGAGGACGGCAGCGTGCAGCTCGCCGACCACTACCA GCAGAACACCCCCATCGGCGACGGCCCCGTGCTGCTGCCCGACAACCACTACC TGAGCACCCAGTCCAAGCTGAGCAAAGACCCCAACGAGAAGCGCGATCACAT GGTCCTGCTGGAGTTCGTGACCGCCGCCGGGATCACTCTCGGCATGGACGAGC TGTACAAGTAA
6x HisTag- LumiScarlet	ATGCATCATCACCATCACCACGTGAGCAAGGGCGAGGCAGTGATCAAGGAGTT CATGCGGTTCAAGGTGCACATGGAGGGCTCCATGAACGGCCACGAGTTCGAGA TCGAGGGCGAGGGCGAGGGCCGCCCCTACGAGGGCACNCAGACCGCCAAGCT GAAGGTGACCAAGGGTGGCCCCCTGCCCTTCTCCTGGGACATCCTGTCCCCTC AGTTCATGTACGGCTCCAGGGCCTTCATCAAGCACCCCGCCGACATCCCCGACT ACTATAAGCAGTCCTTCCCCGAGGGCTTCAAGTGGGAGCGCGTGATGAACTTC GAGGACGGCGGCGCCGTGACCGTGACCCAGGACACCTCCCTGGAGGACGGCA CCCTGATCTACAAGGTGAAGCTCCGCGGCACCAACTTCCCTCCTGACGGCCCC GTAATGCAGAAGAAGACAATGGGCTGGGAAGCGTCCACCGAGCGGTTGTACCC CGAGGACGGCGTGCTGAAGGGCGACATTAAGATGGCCCTGCGCCTGAAGGAC GGCGGCCGCTACCTGGCGGACTTCAAGACCACCTACAAGGCCAAGAAGCCCGT GCAGATGCCCGGCGCCTACAACGTCGACCGCAAGTTGGACATCACCTCCCACA ACGAGGACTACACCGTGGTGGAACAGTACGAACGCTCCGAGGGCCGCCACTCC ACCGGAAAGACTCTCGGGGATTTTGTTGGGGACTGGCGACAGACAGCCGGCTA CAACCAGGCTCAAGTCCTTGAACAGGGAGGTTTGACCAGTTTGTTTCAGAACC TCGGGGTGTCCGTAACTCCAATCCAAAGGATTGTCCTGAGCGGTGAAAATGGG CTGAAGATCGATATCCATGTCATCATCCCGTATGAAGGTCTGAGCTGCGACCAA ATGGCCCAGATCGAAAAAATTTTTAAGGTGGTATACCCTGTGGATGATCATCACT TTAAGGCGATCCTGCACTATGGCACACTGGTAATCGACGGGGTTACGCCGAACA TGATCGACTATTTCGGACAGCCGTATGAAGGCATCGCCAAGTTCGACGGCAAAA AGATCACAGTAACAGGGACCCTGTGGAACGGCAACACAATTATCGACGAGCGC CTGATCAACCCCGACGGCTCCCTGCTGTTCCGAGTAACCATTAACGGAGTGACC GGCTGGCGTCTGCATGAACGCATTCTGGCGTAA

6x HisTag-mScarletI	ATGCATCATCACCATCACCACGTGAGCAAGGGCGAGGCAGTGATCAAGGAGTT CATGCGGTTCAAGGTGCACATGGAGGGCTCCATGAACGGCCACGAGTTCGAGA TCGAGGGCGAGGGCGAGGGCCGCCCCTACGAGGGCACCCAGACCGCCAAGCT GAAGGTGACCAAGGGTGGCCCCCTGCCCTTCTCCTGGGACATCCTGTCCCCTC AGTTCATGTACGGCTCCAGGGCCTTCATCAAGCACCCCGCCGACATCCCCGACT ACTATAAGCAGTCCTTCCCCGAGGGCTTCAAGTGGGAGCGCGTGATGAACTTC GAGGACGGCGGCGCCGTGACCGTGACCCAGGACACCTCCCTGGAGGACGGCA CCCTGATCTACAAGGTGAAGCTCCGCGGCACCAACTTCCCTCCTGACGGCCCC GTAATGCAGAAGAAGACAATGGGCTGGGAAGCGTCCACCGAGCGGTTGTACCC CGAGGACGGCGTGCTGAAGGGCGACATTAAGATGGCCCTGCGCCTGAAGGAC GGCGGCCGCTACCTGGCGGACTTCAAGACCACCTACAAGGCCAAGAAGCCCGT GCAGATGCCCGGCGCCTACAACGTCGACCGCAAGTTGGACATCACCTCCCACA ACGAGGACTACACCGTGGTGGAACAGTACGAACGCTCCGAGGGCCGCCACTCC ACCGGATAA
6x HisTag-LumiLuc	ATGCATCATCACCATCACCACACTCTCGGGGATTTTGTTGGGGACTGGCGACAG ACAGCCGGCTACAACCAGGCTCAAGTCCTTGAACAGGGAGGTTTGACCAGTTT GTTTCAGAACCTCGGGGTGTCCGTAACTCCAATCCAAAGGATTGTCCTGAGCG GTGAAAATGGGCTGAAGATCGATATCCATGTCATCATCCCGTATGAAGGTCTGA GCTGCGACCAAATGGCCCAGATCGAAAAAATTTTTAAGGTGGTATACCCTGTGG ATGATCATCACTTTAAGGCGATCCTGCACTATGGCACACTGGTAATCGACGGGG TTACGCCGAACATGATCGACTATTTCGGACAGCCGTATGAAGGCATCGCCAAGT TCGACGGCAAAAAGATCACAGTAACAGGGACCCTGTGGAACGGCAACACAAT TATCGACGAGCGCCTGATCAACCCCGACGGCTCCCTGCTGTTCCGAGTAACCAT TAACGGAGTGACCGGCTGGCGTCTGCATGAACGCATTCTGGCGTAA
Spacer-LumiScarlet	GGTTCAGGAACAGCAGGTGGTGGGTCAGGTTCCGTGAGCAAGGGCGAGGCAG TGATCAAGGAGTTCATGCGGTTCAAGGTGCACATGGAGGGCTCCATGAACGGC CACGAGTTCGAGATCGAGGGCGAGGGCGAGGGCCGCCCCTACGAGGGCACCC AGACCGCCAAGCTGAAGGTGACCAAGGGTGGCCCCCTGCCCTTCTCCTGGGAC ATCCTGTCCCCTCAGTTCATGTACGGCTCCAGGGCCTTCATCAAGCACCCCGCC GACATCCCCGACTACTATAAGCAGTCCTTCCCCGAGGGCTTCAAGTGGGAGCGC GTGATGAACTTCGAGGACGGCGGCGCCGTGACCGTGACCCAGGACACCTCCCT GGAGGACGGCACCCTGATCTACAAGGTGAAGCTCCGCGGCACCAACTTCCCTC CTGACGGCCCCGTAATGCAGAAGAAGACAATGGGCTGGGAAGCGTCCACCGA GCGGTTGTACCCCGAGGACGGCGTGCTGAAGGGCGACATTAAGATGGCCCTGC GCCTGAAGGACGGCGGCCGCTACCTGGCGGACTTCAAGACCACCTACAAGGCC AAGAAGCCCGTGCAGATGCCCGGCGCCTACAACGTCGACCGCAAGTTGGACAT CACCTCCCACAACGAGGACTACACCGTGGTGGAACAGTACGAACGCTCCGAGG GCCGCCACTCCACCGGAAAGACTCTCGGGGATTTTGTTGGGGACTGGCGACAG ACAGCCGGCTACAACCAGGCTCAAGTCCTTGAACAGGGAGGTTTGACCAGTTT GTTTCAGAACCTCGGGGTGTCCGTAACTCCAATCCAAAGGATTGTCCTGAGCG GTGAAAATGGGCTGAAGATCGATATCCATGTCATCATCCCGTATGAAGGTCTGA GCTGCGACCAAATGGCCCAGATCGAAAAAATTTTTAAGGTGGTATACCCTGTGG ATGATCATCACTTTAAGGCGATCCTGCACTATGGCACACTGGTAATCGACGGGG TTACGCCGAACATGATCGACTATTTCGGACAGCCGTATGAAGGCATCGCCAAGT TCGACGGCAAAAAGATCACAGTAACAGGGACCCTGTGGAACGGCAACACAAT TATCGACGAGCGCCTGATCAACCCCGACGGCTCCCTGCTGTTCCGAGTAACCAT TAACGGAGTGACCGGCTGGCGTCTGCATGAACGCATTCTGGCGTAA

Spacer-mScarletI	GGTTCAGGAACAGCAGGTGGTGGGTCAGGTTCCGTGAGCAAGGGCGAGGCAGTGATCAAGGAGTTCATGCGGTTCAAGGTGCACATGGAGGGCTCCATGAACGGCCACGAGTTCGAGATCGAGGGCGAGGGCGAGGGCCGCCCCTACGAGGGCACCCAGACCGCCAAGCTGAAGGTGACCAAGGGTGGCCCCCTGCCCTTCTCCTGGGACATCCTGTCCCCTCAGTTCATGTACGGCTCCAGGGCCTTCATCAAGCACCCCGCCGACATCCCCGACTACTATAAGCAGTCCTTCCCCGAGGGCTTCAAGTGGGAGCGCGTGATGAACTTCGAGGACGGCGGCGCCGTGACCGTGACCCAGGACACCTCCCTGGAGGACGGCACCCTGATCTACAAGGTGAAGCTCCGCGGCACCAACTTCCCTCCTGACGGCCCCGTAATGCAGAAGAAGACAATGGGCTGGGAAGCGTCCACCGAGCGGTTGTACCCCGAGGACGGCGTGCTGAAGGGCGACATTAAGATGGCCCTGCGCCTGAAGGACGGCGGCCGCTACCTGGCGGACTTCAAGACCACCTACAAGGCCAAGAAGCCCGTGCAGATGCCCGGCGCCTACAACGTCGACCGCAAGTTGGACATCACCTCCCACAACGAGGACTACACCGTGGTGGAACAGTACGAACGCTCCGAGGGCCGCCACTCCACCGGATAA
Spacer-LumiLuc	GGTTCAGGAACAGCAGGTGGTGGGTCAGGTTCCAAGACTCTCGGGGATTTTGTTGGGGACTGGCGACAGACAGCCGGCTACAACCAGGCTCAAGTCCTTGAACAGGGAGGTTTGACCAGTTTGTTTCAGAACCTCGGGGTGTCCGTAACTCCAATCCAAAGGATTGTCCTGAGCGGTGAAAATGGGCTGAAGATCGATATCCATGTCATCATCCCGTATGAAGGTCTGAGCTGCGACCAAATGGCCCAGATCGAAAAAATTTTTAAGGTGGTATACCCTGTGGATGATCATCACTTTAAGGCGATCCTGCACTATGGCACACTGGTAATCGACGGGGTTACGCCGAACATGATCGACTATTTCGGACAGCCGTATGAAGGCATCGCCAAGTTCGACGGCAAAAAGATCACAGTAACAGGGACCCTGTGGAACGGCAACACAATTATCGACGAGCGCCTGATCAACCCCGACGGCTCCCTGCTGTTCCGAGTAACCATTAACGGAGTGACCGGCTGGCGTCTGCATGAACGCATTCTGGCGTAA

Appendix E. Amino acid sequences of cloned constructs

6x HisTag-CeNLuc
MHHHHHHVSKGEELFTGVVPILVELDGDVNGHKFSVSGEGEGDATYGKLTLKFICTTGK
LPVPWPTLVTTLSWGVQCFARYPDHMKQHDFFKSAMPEGYVQERTIFFKDDGNYKTRA
EVKFEGDTLVNRIELKGIDFKEDGNILGHKLEYNAIHGNVYITADKQKNGIKANFGLNCN
IEDGSVQLADHYQQNTPIGDGPVLLPDNHYLSTQSKLSKDPNEKRDHMVLLEFVTAAGI
TLGMDELYKDISGGMVFTLEDFVGDWRQTAGYNLDQVLEQGGVSSLFQNLGVSVTPIQ
RIVLSGENGLKIDIHVIIPYEGLSGDQMGQIEKIFKVVYPVDDHHFKVILHYGTLVIDGVT
PNMIDYFGRPYEGIAVFDGKKITVTGTLWNGNKIIDERLINPDGSLLFRVTINGVTGWRLC
ERILA

Spacer-CeNLuc
GSGTAGGGSGSVSKGEELFTGVVPILVELDGDVNGHKFSVSGEGEGDATYGKLTLKFICT
TGKLPVPWPTLVTTLSWGVQCFARYPDHMKQHDFFKSAMPEGYVQERTIFFKDDGNYK
TRAEVKFEGDTLVNRIELKGIDFKEDGNILGHKLEYNAIHGNVYITADKQKNGIKANFGL
NCNIEDGSVQLADHYQQNTPIGDGPVLLPDNHYLSTQSKLSKDPNEKRDHMVLLEFVTA
AGITLGMDELYKDISGGMVFTLEDFVGDWRQTAGYNLDQVLEQGGVSSLFQNLGVSVT
PIQRIVLSGENGLKIDIHVIIPYEGLSGDQMGQIEKIFKVVYPVDDHHFKVILHYGTLVIDG
VTPNMIDYFGRPYEGIAVFDGKKITVTGTLWNGNKIIDERLINPDGSLLFRVTINGVTGWR
LCERILA

6x His Tag- mCerulean3
HHHHHHVSKGEELFTGVVPILVELDGDVNGHKFSVSGEGEGDATYGKLTLKFICTTGKL
PVPWPTLVTTLSWGVQCFARYPDHMKQHDFFKSAMPEGYVQERTIFFKDDGNYKTRAE
VKFEGDTLVNRIELKGIDFKEDGNILGHKLEYNAIHGNVYITADKQKNGIKANFGLNCNI
EDGSVQLADHYQQNTPIGDGPVLLPDNHYLSTQSKLSKDPNEKRDHMVLLEFVTAAGIT
LGMDELYK

Spacer-mCerulean3
GSGTAGGGSGSVSKGEELFTGVVPILVELDGDVNGHKFSVSGEGEGDATYGKLTLKFICT
TGKLPVPWPTLVTTLSWGVQCFARYPDHMKQHDFFKSAMPEGYVQERTIFFKDDGNYK
TRAEVKFEGDTLVNRIELKGIDFKEDGNILGHKLEYNAIHGNVYITADKQKNGIKANFGL
NCNIEDGSVQLADHYQQNTPIGDGPVLLPDNHYLSTQSKLSKDPNEKRDHMVLLEFVTA
AGITLGMDELYK

6x His Tag-LumiScarlet

MHHHHHHVSKGEAVIKEFMRFKVHMEGSMNGHEFEIEGEGEGRPYEGTQTAKLKVTK
GGPLPFSWDILSPQFMYGSRAFIKHPADIPDYYKQSFPEGFKWERVMNFEDGGAVTVTQ
DTSLEDGTLIYKVKLRGTNFPPDGPVMQKKTMGWEASTERLYPEDGVLKGDIKMALRL
KDGGRYLADFKTTYKAKKPVQMPGAYNVDRKLDITSHNEDYTVVEQYERSEGRHSTG
KTLGDFVGDWRQTAGYNQAQVLEQGGLTSLFQNLGVSVTPIQRIVLSGENGLKIDIHVII
PYEGLSCDQMAQIEKIFKVVYPVDDHHFKAILHYGTLVIDGVTPNMIDYFGQPYEGIAKF
DGKKITVTGTLWNGNTIIDERLINPDGSLLFRVTINGVTGWRLHERILA

6x His Tag-LumiLuc

MHHHHHHTLGDFVGDWRQTAGYNQAQVLEQGGLTSLFQNLGVSVTPIQRIVLSGENGL
KIDIHVIIPYEGLSCDQMAQIEKIFKVVYPVDDHHFKAILHYGTLVIDGVTPNMIDYFGQP
YEGIAKFDGKKITVTGTLWNGNTIIDERLINPDGSLLFRVTINGVTGWRLHERILA

6x His Tag-mScarletI

MHHHHHHVSKGEAVIKEFMRFKVHMEGSMNGHEFEIEGEGEGRPYEGTQTAKLKVTK
GGPLPFSWDILSPQFMYGSRAFIKHPADIPDYYKQSFPEGFKWERVMNFEDGGAVTVTQ
DTSLEDGTLIYKVKLRGTNFPPDGPVMQKKTMGWEASTERLYPEDGVLKGDIKMALRL
KDGGRYLADFKTTYKAKKPVQMPGAYNVDRKLDITSHNEDYTVVEQYERSEGRHSTG

Spacer-LumiScarlet

GSGTAGGGSGSVSKGEAVIKEFMRFKVHMEGSMNGHEFEIEGEGEGRPYEGTQTAKLKV
TKGGPLPFSWDILSPQFMYGSRAFIKHPADIPDYYKQSFPEGFKWERVMNFEDGGAVTVT
QDTSLEDGTLIYKVKLRGTNFPPDGPVMQKKTMGWEASTERLYPEDGVLKGDIKMALR
LKDGGRYLADFKTTYKAKKPVQMPGAYNVDRKLDITSHNEDYTVVEQYERSEGRHSTG
KTLGDFVGDWRQTAGYNQAQVLEQGGLTSLFQNLGVSVTPIQRIVLSGENGLKIDIHVII
PYEGLSCDQMAQIEKIFKVVYPVDDHHFKAILHYGTLVIDGVTPNMIDYFGQPYEGIAKF
DGKKITVTGTLWNGNTIIDERLINPDGSLLFRVTINGVTGWRLHERILA

Spacer-LumiLuc

GSGTAGGGSGSTLGDFVGDWRQTAGYNQAQVLEQGGLTSLFQNLGVSVTPIQRIVLSGE
NGLKIDIHVIIPYEGLSCDQMAQIEKIFKVVYPVDDHHFKAILHYGTLVIDGVTPNMIDYF
GQPYEGIAKFDGKKITVTGTLWNGNTIIDERLINPDGSLLFRVTINGVTGWRLHERILA

Spacer- mScarletI

GSGTAGGGSGSVSKGEAVIKEFMRFKVHMEGSMNGHEFEIEGEGEGRPYEGTQTAKLKV
TKGGPLPFSWDILSPQFMYGSRAFIKHPADIPDYYKQSFPEGFKWERVMNFEDGGAVTVT
QDTSLEDGTLIYKVKLRGTNFPPDGPVMQKKTMGWEASTERLYPEDGVLKGDIKMALR
LKDGGRYLADFKTTYKAKKPVQMPGAYNVDRKLDITSHNEDYTVVEQYERSEGRHSTG
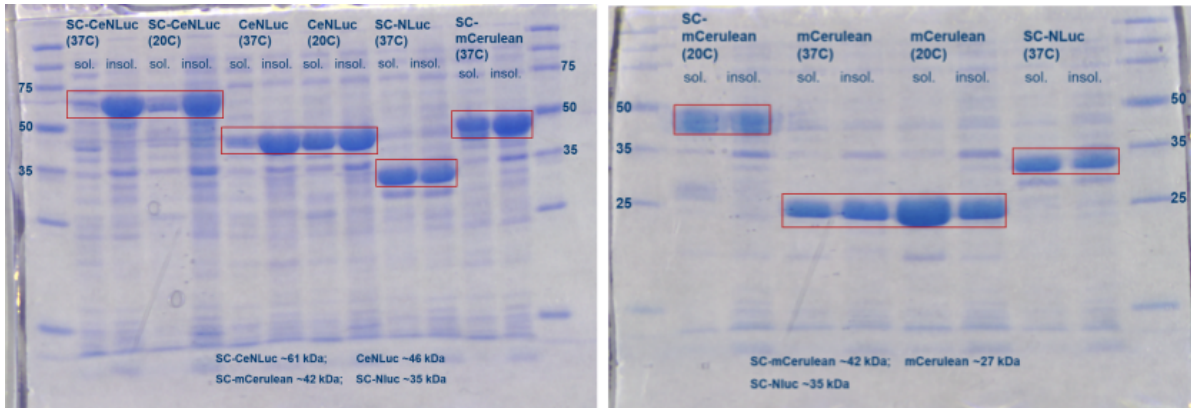
Appendix F. Supplementary figures

Figure S1. Expression of SC-CeNLuc, CeNLuc, SC-mCerulean, and mCerulean at incubation temperatures of 37°C for 3 hours or 20°C for 16 hours with 1mM IPTG. Soluble and insoluble fractions of cell lysates were run. SC-Nluc, which was previously expressed in the lab, was run as a control.
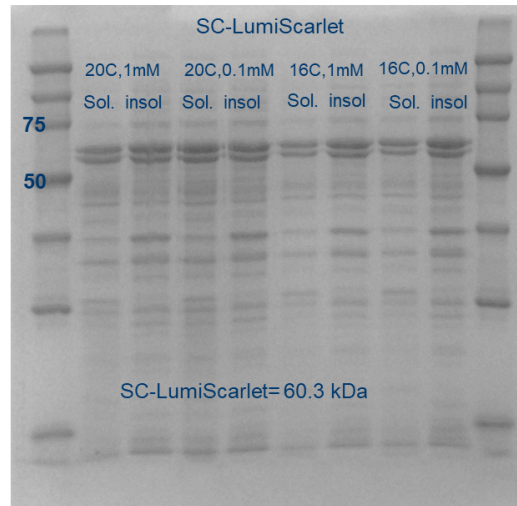

Figure S2. SC-LumiScarlet expression optimization. Expression was induced at incubation conditions of 16 or 20°C with 0.1 or 1mM IPTG and after expression cells were collected. Cell lysates were separated for soluble and insoluble fractions and all fractions were run on SDS-PAGE. More soluble fraction was observed for protein expressed at 20°C incubation induced with 0.1 mM IPTG.
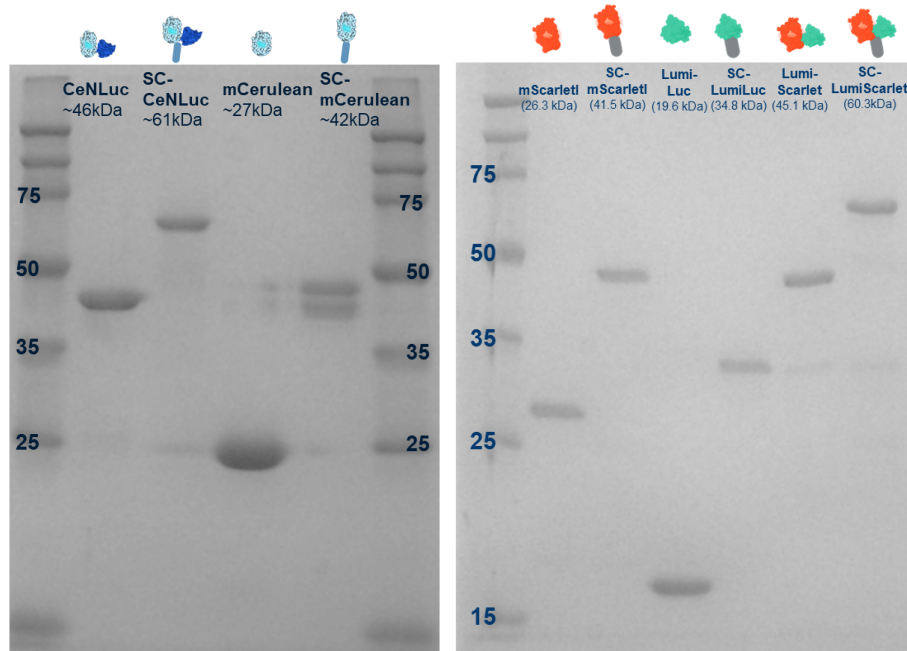
Figure S3. Final Purified Proteins. The purified proteins were run on SDS-PAGE and molecular weights were confirmed to align with the expected weights of the proteins.
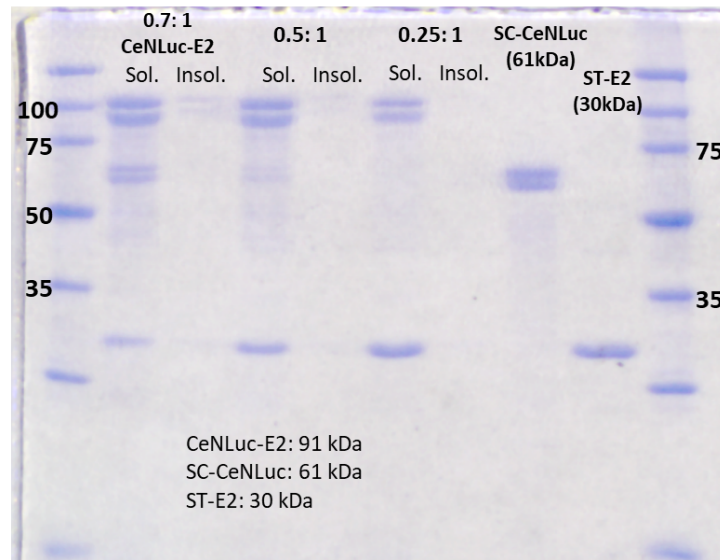

Figure S4. CeNLuc-E2 conjugation at conjugation ratios of 0.7:1, 0.5:1, and 0.25:1 SC-CeNLuc to ST-E2 subunit. For the particles, bands around 30 kDa indicate unconjugated ST-E2 monomers and bands around 90 kDa indicate monomers conjugated with SC-CeNLuc. Additionally, for particles with incomplete conjugation of SC-CeNLuc, a third band is present around 60 kDa.
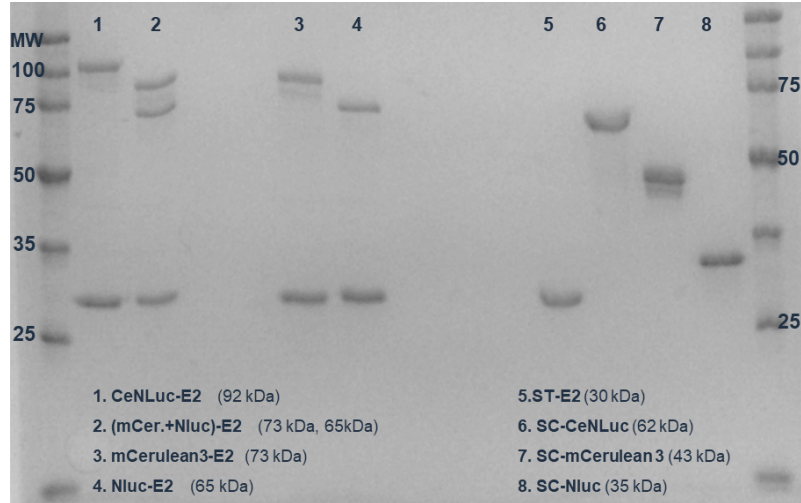
Figure S5. SDS-PAGE of CeNLuc-E2, (mCerulean3+Nluc)-E2, mCerulean3-E2, and Nluc-E2 conjugations. A conjugation ratio of 0.25 moles luminescent protein to 1 mole ST-E2 subunit was used. For the conjugated particles, bands around 30 kDa indicate unconjugated ST-E2 monomors, and bands greater than 30 kDa indiciate ST-E2 monomors conjugated with luminescent protein. Lane 2 contains two bands greater than 30 kDa indicating the conjugation of both SC-mCerulean3 and SC-Nluc.
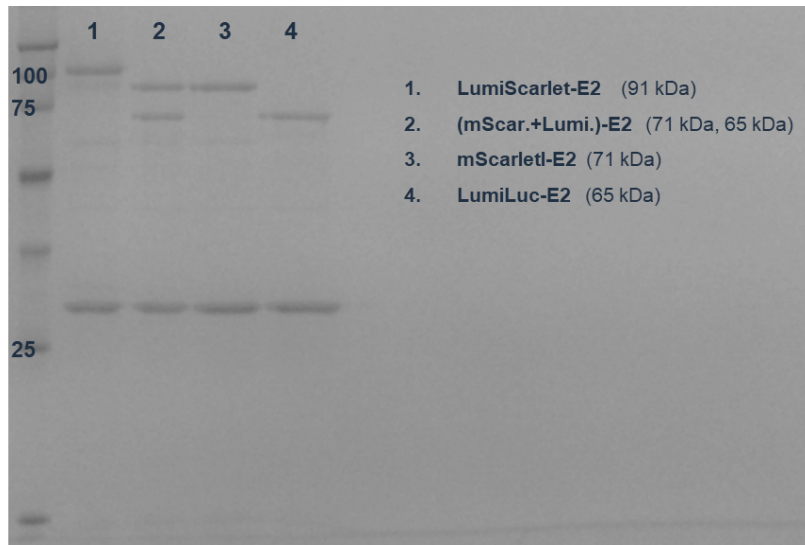

Figure S6. SDS-PAGE of LumiScarlet-E2, (mScarletI+LumiLuc)-E2, mScarletI-E2, LumiLuc-E2 conjugations. A conjugation ratio of 0.25 moles luminescent protein to 1 mole ST-E2 subunit was used. For the conjugated particles, bands around 30 kDa indicate unconjugated ST-E2 monomors, and bands greater than 30 kDa indiciated ST-E2 monomors conjugated with luminescent protein. Lane 2 contains two bands greater than 30 kDa indicating the conjugation of both SC-mScarletI and SC-LumiLuc.
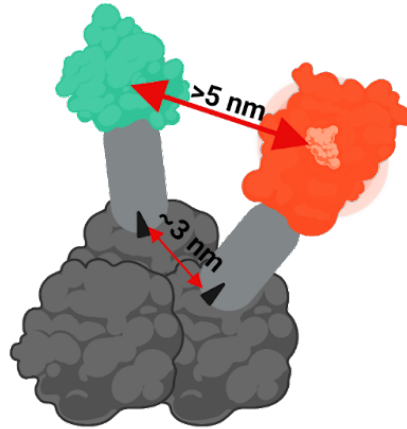
Figure S7. Rendering of the closest distance a SC-fluorescent protein and SC-bioluminescent protein can conjugate on a trimer of ST-E2. The closest distance between the SpyCatcher proteins is around 3 nm, while the closest distance between the chromophores of the fluorescent and bioluminescent protein is estimated to be greater than 5 nm. Components drawn to scale and based on published protein structures. Protein Data Bank ID codes 1B5S (E2), 4MLI (SpyCatcher), 4EN1 (mCerulean3), 5LK4 (mScarletI), 5IBO (Nluc).
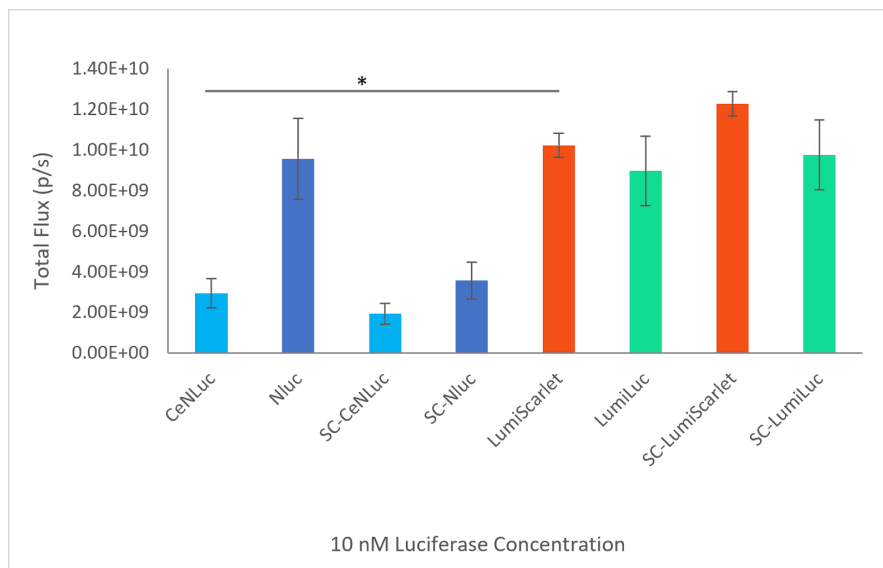

Figure S8. Comparison of the total luminescence of all soluble luminescent proteins containing Nluc or LumiLuc. Measurements were performed in triplicates and data are represented as mean± SEM with background subtracted. One-way ANOVA with Tukey's multiple comparison test were performed (*$p < 0.05$).
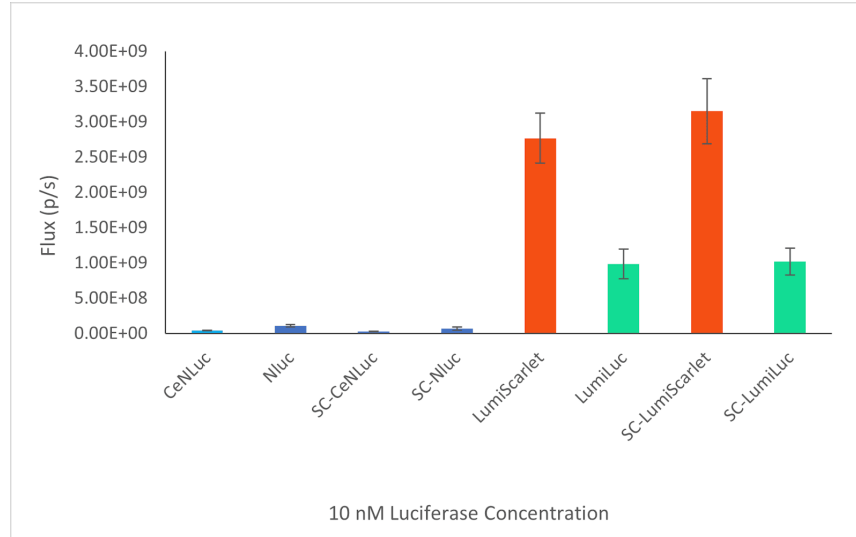
Figure S9. Comparison of the DsRed emission of all soluble luminescent proteins containing Nluc or LumiLuc. Measurements were performed in triplicates and data are represented as mean± SEM with background subtracted.